Multi-Objective Multistage Distributionally Robust Flexibility Enhancement for Seaport Logistic-Energy Coordination

Multi-Objective Multistage Distributionally Robust Flexibility Enhancement for Seaport Logistic-Energy Coordination

Yiwen Huang, Wentao Huang, *Senior Member, IEEE,* Tao Huang, *Senior Member, IEEE,* Canbing Li, *Senior Member, IEEE,* Ran Li, *Member, IEEE,* Nengling Tai, *Senior Member, IEEE,* Ettore Francesco Bompard

***Abstract*—Logistic-energy coordination is an effective way to improve energy efficiency for electrified seaports. However, exiting works adopt fixed logistic power load models and seldom address renewable energy uncertainty adequately, resulting in low system flexibility and robustness. In this paper, a novel logistic-energy collaborative dispatch model is first proposed. The model integrates energy feedback from all-electric ships (AESs) and electric-powered cranes as well as automated guided vehicles (AGVs) battery swapping mode into entire logistic-energy coordination process. Logistic-side flexibility provision is significantly enhanced by variable bidirectional power flows and win-win battery swapping. Then a multi-objective multistage distributionally robust optimization (MMDRO) framework is established to address renewable energy uncertainty. This enables a trade-off between multiple objectives while ensuring solution non-anticipativity, economics and robustness via multi-stage distributionally robust optimization (DRO). The MMDRO is intractable due to multi-objectives, mixed-integer property and nested min-max-min optimization structure. To this end, an improved multi-objective stochastic dual dynamic integer programming (SDDiP) algorithm with controllable convergence process and two-step weight update is developed to effectively solve the model. Case studies demonstrate the superiority of our approach over existing methods.**

***Index Terms*—Logistic-energy coordination, seaport power distribution network, multi-objective multistage distributionally robust optimization, flexibility enhancement.**

NOMENCLATURE

Abbreviations

SPDN	Seaport power distribution network
AES	All-electric ship
QC	Quay crane
ESS	Energy storage system
AGV	Automated guided vehicle
SP	Stochastic programming
RO	Robust optimization
DRO	Distributionally robust optimization
SDDP	Stochastic dual dynamic programming
SDDiP	Stochastic dual dynamic integer programming
RDDP	Robust dual dynamic programming
LP	Linear programming
MIP	Mixed integer programming
MMDRO	Multi-objective multistage distributionally robust optimization

Indices and Sets

b, $\mathcal{B}$	Index/set of berths
s, $\mathcal{S}$	Index/set of AESs
q, $\mathcal{Q}$	Index/set of QCs
n, $\mathcal{N}$	Index/set of batteries
v, $\mathcal{V}$	Index/set of AGVs
t, $\mathcal{T}$	Index/set of time periods
m	Index of renewable energy unit
i, j, k	Index of electric node of SPDN

Parameters

B^{max}, Q^{max}	Number of available berths and QCs
$Q_s^{min/max}$	Minimum/maximum number of QCs that can be assigned for AES s
t_s^a, $t_s^{d,max}$	Arrival and latest departure time of AES s
$P_{(\cdot)}^{(\cdot),\min/\max}$	Minimum/maximum power limits
$\beta_{s,(\cdot)}^{AES}$	Generation coefficients of auxiliary generator on AES s
P_s^{SL}	Service load of AES s
$\eta_{(\cdot)}^{(\cdot),ch/dis}$	Charging/discharging efficiency of ESS and battery
$d_{s/q/n}^{AES/QC/BT}$	Degradation cost coefficients of ESS and battery
$E_{(\cdot)}^{(\cdot),\min/\max}$	Minimum/maximum energy limits of ESS and battery
$E_s^{AES,Req}$	Required energy level of ESS on AES s when the AES departs seaport
TEU_s^{Req}	Total number of cargoes that need to be handled on AES s
$\Delta t_q^{up/down}$	Duration of lifting up/down in one cargo handling cycle of QC q
$P_q^{QC,up}$	Power load of QC q when lifting up
$P_q^{QC,down,\max}$	Available regenerated power of QC q when lifting down
$\eta_q^{QC,max}$	Maximum cargo handling efficiency of QC q
$\eta_v^{AGV,(\cdot),\max}$	Maximum cargo transport efficiency of AGV v when working and swapping battery
ΔE_v^{AGV}	Energy consumption of battery on AGV n in one cargo transport cycle
$\underline{E}_n^{BSS,swapin}$	Required energy level of battery n when being put into AGV
$\overline{E}_n^{BSS,swapout}$	Required energy level of battery n when being removed from AGV

Manuscript received 18 December 2023; revised 19 March 2024; accepted 23 April 2024. This work was supported by National Natural Science Foundation of China (U2243243, 52337006), Program of Shanghai Academic Research Leader (22XD1401400). (*Corresponding author: Wentao Huang*)

Yiwen Huang, Wentao Huang, Canbing Li, Ran Li, Nengling Tai are with the Key Laboratory of Control of Power Transmission and Conversion, Ministry of Education, Shanghai Jiao Tong University, Shanghai 200240, China (e-mail: hyw1998@sjtu.edu.cn; hwt8989@sjtu.edu.cn; licanbing@sjtu.edu.cn; rl272@sjtu.edu.cn; nltai@sjtu.edu.cn).

Tao Huang, and Ettore Francesco Bompard are with the Department of Energy, Politecnico di Torino, Torino 10129, Italy (e-mail: tao.huang@polito.it; ettore.bompard@polito.it).

$c_t^{grid,DA}$ Day-ahead electricity purchase cost coefficient at time t

$c_t^{grid,ID,+/-}$ Intra-day electricity adjustment cost coefficients at time t

$P_{j,t}^{load}$, $Q_{j,t}^{load}$ Constant electricity load at node j at time t

$P_{m,t}^{RES,f}$ Forecast output of renewable energy unit m at time t

Decision Variables

X_{bst}, ω_{qst} Status indicator of AES s and QC q at time t

B_s, t_s^b, t_s^d Berthing location, berthing start time and departure time of AES s

$P_{s,t}^{G2S}$, $P_{s,t}^{S2G}$ Power flows from SPDN to AES s and AES s to SPDN at time t

$u_{s,t}^{AG}$, $P_{s,t}^{AG}$ Status indicator and power output of auxiliary generators on AES s at time t

$P_{(\cdot),t}^{(\cdot),ch/dis}$ Charging/discharging power of ESS and battery at time t

$E_{(\cdot),t}^{(\cdot),ch/dis}$ Energy level of ESS and battery at time t

$TEU_{s,t}$ Cargoes that have been handled on AES s until time t

$P_{q,t}^{G2Q}$, $P_{q,t}^{Q2G}$ Power flows from SPDN to QC q and QC q to SPDN at time t

$\eta_{q,t}^{QC}$ Cargo handling efficiency of QC q at time t

$\eta_{v,q,t}^{AGV,(\cdot)}$ Cargo transport efficiency of AGV v serving for QC q at time t when working and swapping battery

$\hat{P}_{q,t}^{QC,down}$ Utilized regenerated power of QC q at time t

$I_{(\cdot)}^{(\cdot)}$, $\delta_{(\cdot)}^{(\cdot)}$, $\sigma_{(\cdot)}^{(\cdot)}$ Status indicator of AGV and battery

$P_{ij,t}^{line}$, $Q_{ij,t}^{line}$ Active and reactive power flows from node i to node j at time t

$P_{m,t}^{RES}$ Utilized renewable output of unit m at time t

$U_{j,t}$ Voltage magnitude of node j at time t

I. Introduction

DUE to ambitious decarbonization targets in the maritime sector, the electrification of seaports has become an irreversible trend [1]. Various green technologies, such as cold-ironing [2], all-electric ships (AESs) [3], electric-powered logistic equipment [4], renewable energy [5], energy storage systems (ESSs) [6], and integrated energy [7], are now incorporated into seaports. In this context, the logistics system is connected to the seaport distribution network (SPDN) and serves as its load side. The energy management of electrified seaports transforms into a complex logistics-energy coordination problem, especially in uncertain operational conditions due to the intermittent renewable energy sources.

Traditionally, the logistics system and the SPDN are scheduled independently of each other. On the one hand, the logistic operation, including berth allocation [8], quay crane assignment [9], automated guided vehicles (AGVs) dispatch [10] and their joint scheduling [11], [12], generally ignore the associated energy consumption and the potential impact on the SPDN. However, in electrified seaports, the impact can no longer be neglected because logistic scheduling directly determines the power demand of the logistic system, subsequently affecting SPDN operations. On the other hand, the SPDN dispatch generally assumes exogenously specified logistic schemes [13], [14]. This means that the total power demands of seaport equipment are predetermined and their logistical characteristics are completely disregarded, leading to low system flexibility.

To realize better energy management, logistic-energy collaborative dispatch has emerged as a new research line in recent years. The fundamental idea is to realize temporal and spatial shifting of logistic power loads, known as logistic-side demand response. In current publications, this is typically achieved by changing logistics operation schemes. Reference [15] proposes the optimal scheduling for seaport integrated energy systems, where the temporal power loads of AESs are flexibly adjusted by changing AES's berthing duration. In [16], an optimal voltage control method is developed to mitigate voltage violations in the seaport distribution network (SPDN) by coordinating AES berthing decisions. In [17], both AES berth allocation and quay crane (QC) assignment are coordinated with the seaport smart grid. In [18], a comprehensive logistic-energy collaborative dispatch model is developed, where AESs, QCs, electric/hydrogen-powered AGVs, and reefer containers are formulated to participate in logistic-side demand response. Furthermore, our previous work [19] explicitly formulates the time and space properties of logistic-energy coordination process and develops a multistage robust dynamic scheduling framework to address involved multiple uncertainties.

The aforementioned works have made remarkable progress in the field. However, several unresolved issues remain:

1) Regarding model formulation, all these works adopt fixed logistic power load models. This implies that the rated power of AESs and logistic equipment is constant, and their demands are formulated as the product of logistic status (denoted by binary variables) and rated power. While this modeling method is valid, it may be considered rigid since logistic-side demand response can only be achieved by adjusting logistic operation schemes. The coordination benefit is highly dependent on how long AESs can stay in the seaport and may be limited if AESs aim to leave the seaport as soon as possible. Moreover, the majority of previous works exclusively concentrate on the flexibility provision of AESs and QCs, overlooking another crucial logistic component, that is, the AGV scheduling.

2) Concerning dispatch strategy, most of these works implement deterministic optimization without considering renewable energy uncertainty or adopt simple methods to handle them. However, the output of renewable energy determines the power supply of SPDN, thereby exerting a significant influence on logistic system management on the load side. Ignoring the renewable energy uncertainty will aggravate the supply-demand mismatch and diminish the practical benefits of collaborative dispatch.

For the first issue, recent publications have highlighted some advanced techniques that enable logistic equipment to exhibit a variable net power demand and even feed energy back to SPDNs. Cranes equipped with energy storage systems (ESSs), for instance, can harvest and store regenerated braking energy when lowering cargoes [20], [21]. The stored energy can support hoist lifts and be fed back to SPDNs when needed. In this case, the net power demands of cranes are no longer fixed but variable and bidirectional. Furthermore, the Ship-to-Grid (S2G) technology allows berthed AESs to provide power for SPDNs, supporting onshore energy scheduling [22], [23]. With these technologies, system flexibility

TABLE I
COMPARISON OF PREVIOUS PUBLICATIONS AND OUR WORK

Reference	Logistic-side demand response resources			Uncertainties handling	Multiple objectives
	AES	QC	AGV		
[15]	Berth allocation	No	No	No	No
[16]	Berth allocation	No	No	No	No
[17]	Berth allocation	Assignment	No	Two-stage SP	No
[18]	Berth allocation	Assignment	Battery charging	No	Yes
[19]	Berth allocation	Assignment	No	Multistage RO	No
Proposed	Berth allocation + energy feedback	Assignment + energy feedback	Battery swapping	Multistage DRO	Yes

can be further enhanced through dual responses through adjustments in both logistics operation schemes and basic power profiles. Unfortunately, existing literature primarily concentrates on the short-term control of these technologies, paying little attention to their operation models and integration with entire logistic-energy coordination process.

Moreover, serving as a link between the terminal and yard, AGVs play a crucial role in seaport logistic scheduling. Reference [24] explores charging mode-based AGV scheduling. However, logistic efficiency may be hindered as AGVs cannot be scheduled during charging. In contrast, the AGV battery swapping mode, widely adopted in many real-world seaports, offers a win-win situation for both logistic efficiency and SPDN management. The battery swapping process takes only minutes, ensuring minimal downtime for logistic operations, while the idle batteries in the battery swapping station (BSS) can be strategically scheduled to support SPDN dispatch. Despite these benefits, existing publications focus solely on the logistic scheduling of AGV battery swapping in seaports [24], overlooking battery energy management and its interaction with SPDN. The integration of AGV battery swapping mode into logistics-energy coordination remains an unexplored research gap.

For the second issue, three common approaches in literature to address uncertainty are stochastic programming (SP) [25], robust optimization (RO) [26], and distributionally robust optimization (DRO) [27]. Among them, DRO stands out as it neither requires exact probability information nor seeks a worst-case scenario solution. Typically, these three methods are implemented in a two-stage framework, where the first-stage solution is made assuming that the uncertainties at each time period of the second stage are revealed simultaneously. However, in practice, uncertainties are sequentially observed over time, and dispatch decisions are made period-by-period based on the revealed uncertainty. This temporal logic and causality are referred to as non-anticipativity [28]. Given that energy constraints of energy storage systems (ESSs) and cargo handling constraints connect adjacent stages, logistics-energy coordination should be implemented in a multistage framework. Multistage scheduling ensures that current decisions are based only on previous uncertainties, thereby enforcing non-anticipativity in solutions. Reference [29] developed a multistage SP model for a grid-connected microgrid using stochastic dual dynamic programming (SDDP). To handle binary/integer variables, stochastic dual dynamic integer programming (SDDiP) was proposed in [30]. Based on this, a combined method integrating Benders decomposition and SDDiP is developed in [31] for the retrofit planning and flexible operation of coal-fired units. In [32], a fast robust dual dynamic programming (RDDP) with efficient approximation of high-dimensional convex hull and adaptive stage selection strategy is developed to accelerates the computation of large-scale economic dispatch problems. In [33], a multistage robust resilience enhancement strategy is designed for distribution systems using modified RDDP algorithm. Reference [34] designed a multi-stage distributionally robust SDDP method for multi-period economic dispatch problems with virtual energy storage. In [35], a multistage distributionally robust scheduling model is developed for hydro–wind–solar systems considering multiple time-scale uncertainties. In [36], a multistage DRO model was proposed to address endogenous and exogenous uncertainties in generation dispatch problems.

The aforementioned works have contributed to the multistage scheduling, yet they focus solely on a single optimization objective. This is insufficient for seaports, as at least two objectives, such as logistic efficiency and energy cost, are involved in the system. In this regard, multistage scheduling should expand to multiple objectives for seaports. Nevertheless, existing literature on this subject is quite limited. Reference [37] introduces a multi-objective SDDP algorithm, but it is designed for linear programming (LP) problems and not applicable to seaport mixed-integer models. Furthermore, the convergence criterion of the algorithm is the same as that of SDDP. Due to random sampling of SDDP, upper bound (UB) is volatile and convergence process is uncontrollable to some extent. As a result, it is difficult to decide in which iteration the solution obtained is truly optimal, and worse, the algorithm may terminate prematurely before finding the genuinely optimal solution. Moreover, the results obtained after each run of the algorithm may differ due to the inherent random process. This lack of reproducibility can be challenging for real-world engineering applications.

In summary, the above literature review illustrates the following research gaps: i) Current logistic-energy coordination models are not flexible enough due to adopting fixed logistic power load models and considering only part of logistics components; ii) Most works ignore the uncertainties associated with renewable energy or adopt simple uncertainty handling methods. iii) Majority of multistage scheduling is single objective-based, while the exiting multi-objective multistage scheduling algorithm is designed only for LP problems and exhibits certain shortcomings in terms of convergence performance. A detailed comparison of previous publications and our work is provided in Table I. To address these gaps, this paper proposes enhancing flexibility for seaport logistic-energy coordination by focusing on model

formulation, uncertainty handling framework and solution algorithm. The main contributions of this paper include:

1) A novel logistic-energy collaborative dispatch model is proposed, which integrates energy feedback of AES and QC as well as AGV battery swapping into entire logistic-energy coordination process. Comparing to exiting models, the proposed model achieves more comprehensive and flexible logistic-side demand response through logistic scheme adjustment, variable bidirectional logistic power loads and win-win AGV battery swapping mode.

2) To address renewable energy uncertainty, a multi-objective multistage distributionally robust optimization (MMDRO) scheduling framework is established. The approach allows for the implementation of multiple objectives to meet the diverse operational requirements of seaports while ensuring solution non-anticipativity, economics, and robustness through multistage DRO.

3) An improved multi-objective SDDiP algorithm is developed to effectively solve MMDRO. On the one hand, the algorithm procedure is redesigned to achieve a controllable and deterministic convergence process, facilitating finding truly optimal solutions and ensuring reproducibility in real-world projects. Required by that, the over-approximation of saddle cost-to-go function and its calculation method are analytically derived. On the other hand, a two-step weight update method is developed to handle the mixed-integer property of logistic-energy coordination model.

In the rest, Section II formulates logistic-energy collaborative dispatch model. Section III establishes MMDRO framework. Section IV presents solution algorithm. Section V gives numerical results. Section VI concludes this paper.

II. LOGISTIC-ENERGY COLLABORATIVE DISPATCH MODEL

A. Problem Background

Fig. 1 shows the connection between SPDN and logistic system. The berthed AESs, electric-powered QCs and BSS are linked with certain nodes of SPDN. The SPDN is responsible for supporting logistics system operations by purchasing electricity from the upstream grid and utilizing renewable energy. The target of logistic system is to complete cargo handling tasks before AESs leave. In the process, arrival AESs first wait at anchorage and then start berthing at allocated berths after receiving scheduling signals from the seaport, known as berth allocation. Simultaneously, several QCs are assigned to the berthed AES for cargo handling, and the cargoes are subsequently transported from the terminal to the yard by AGVs. The AGV will be scheduled to swap battery in the BSS when the equipped battery is exhausted.

The logistics operation schemes determine the profile of logistic power loads. For instance, the berthing location of AES directly influences which electric node is loaded and the related QC assignment, which subsequently affects the spatial distribution of their power loads. Additionally, the berthing duration of AES impacts the temporal distribution of its own load and the associated QC loads. The situation becomes more complex when the energy feedback of AESs and QCs are considered. Although AGVs are not directly connected to the SPDN, their scheduling determines the timing of swapping battery, further affecting the charging/discharging of batteries in the BSS. Therefore, it is essential to coordinate the entire logistic process with SPDN to achieve better energy management and efficiency.

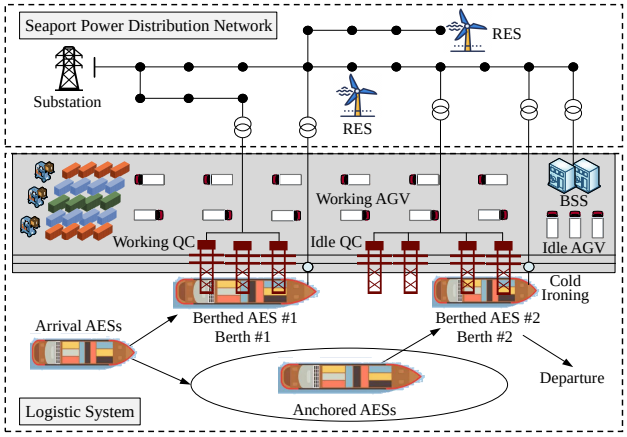

Fig. 1. Illustration of connection between SPDN and logistic system.

B. Model Formulation

In this subsection, the mathematical formula of logistic-energy collaborative dispatch model is provided, with detailed modeling of each logistic component, SPDN and their jointly scheduling.

1) Modeling of AES: The berthing status of AES is represented by a three-dimensional binary variable $X_{b,s,t}$, which equals 1 if AES s is berthing at berth b at time t, otherwise it is 0. Equation (1) links $X_{b,s,t}$ to berthing location B_s and berthing duration $\left[t_s^b, t_s^d\right]$.

$$X_{b,s,t} = \begin{cases} 1, \text{ if } b = B_s \ \& \ t \in \left[t_s^b, t_s^d\right] \\ 0, \text{ otherwise} \end{cases} \tag{1}$$

Using big-M method [38], equation (1) is linearized as:

$$bX_{b,s,t} \le B_s \tag{2.1}$$

$$bX_{b,s,t} + M\left(1 - X_{b,s,t}\right) \ge B_s \tag{2.2}$$

$$tX_{b,s,t} \le t_s^d \tag{2.3}$$

$$tX_{b,s,t} + M\left(1 - X_{b,s,t}\right) \ge t_s^b \tag{2.4}$$

$$\sum_{b\in\mathcal{B}}\sum_{t\in\mathcal{T}} X_{b,s,t} \ge t_s^d - t_s^b + 1 \tag{2.5}$$

The berth allocation constraints are formulated as:

$$t_s^a \le t_s^b, \quad t_s^b \le t_s^d \le t_s^{d,\max} \tag{3.1}$$

$$1 \le B_s \le B^{\max} \tag{3.2}$$

$$\sum_{b\in\mathcal{B}} X_{b,s,t} \le 1, \quad \sum_{s\in\mathcal{S}} X_{b,s,t} \le 1 \tag{3.3}$$

$$\sum_{b\in\mathcal{B}}\sum_{t\in\mathcal{T}} X_{b,s,t} \ge \left\lceil \frac{TEU_s^{Req}}{Q_s^{\max}\eta_q^{QC,\max}} \right\rceil \tag{3.4}$$

Constraints (3.1)-(3.2) restrict berthing duration and berthing location within allowable ranges. Constraint (3.3) ensures that each AES can only be assigned to one berth, and each berth can only serve at most one AES at any time. Constraint (3.4) specifies the minimum berthing duration based on maximum cargo handling efficiency, where $\lceil\cdot\rceil$ means rounding up.

The berthed AES is powered by onshore electricity from the SPDN. In the literature, the power load of AES is denoted as $\sum_{b\in\mathcal{B}} X_{b,s,t} P_s^{AES}$, where P_s^{AES} represents the constant AES power demand including service load and charging power of onboard ESSs [16]. This expression defines a fixed unidirectional power load model, implying that the demand response of AES can solely be achieved by changing its berthing status $X_{b,s,t}$. However, this approach is considered rigid and ignores the potential capacity of AES to adjust its power load.

In this study, we take into account the participation of AES power systems equipped with onboard ESSs and auxiliary generators [39]. The onboard ESSs can discharge to meet AES service load or support the SPDN. The auxiliary generators are typically shut down most of the time to avoid carbon emissions, while the energy feedback mainly comes from onboard ESSs. However, when necessary, such as when the SPDN voltage exceeds its limit, the auxiliary generators will start up to provide electricity supports. This significantly improves the system's ability to withstand operation risks while avoiding excessive carbon emissions from AES. Such setting can be achieved by assigning appropriately large values to the cost coefficients of generators in the objective function (10.4). Consequently, the net power loads of AESs are not fixed and unidirectional but rather variable and bidirectional. The flexibility arises from the power load adjustment and energy feedback of AESs. It expands the demand response of AESs, stemming not only from berth allocation adjustments but also from variable bidirectional energy flow between AESs and the SPDN. Given this concept, the AES onboard power system is formulated by considering the following power balance condition:

$$\left(P_{s,t}^{G2S} - P_{s,t}^{S2G}\right) + P_{s,t}^{AES,dis} + P_{s,t}^{AG} = P_{s,t}^{AES,L} + P_{s,t}^{AES,ch} \tag{4.1}$$

where the power exchange between AES power system and SPDN is defined by the difference between two positive variables $P_{s,t}^{G2S} - P_{s,t}^{S2G}$. This can be regarded as the net power load of AES, which is positive when SPDN delivers power to AES, otherwise, AES feeds energy back to SPDN.

Equation (4.1) holds only during AES berthing. Thus the following constraints should be added:

$$\begin{aligned}\sum_{b\in\mathcal{B}} X_{b,s,t} P_s^{G2S/S2G,\min} &\le P_{s,t}^{G2S/S2G} \\ &\le \sum_{b\in\mathcal{B}} X_{b,s,t} P_s^{G2S/S2G,\max}\end{aligned} \tag{4.2}$$

$$\begin{aligned}\sum_{b\in\mathcal{B}} X_{b,s,t} P_s^{AES,ch/dis,\min} &\le P_{s,t}^{AES,ch/dis} \\ &\le \sum_{b\in\mathcal{B}} X_{b,s,t} P_s^{AES,ch/dis,\max}\end{aligned} \tag{4.3}$$

$$\begin{cases} 0 \le u_{s,t}^{AG} \le \sum_{b\in\mathcal{B}} X_{b,s,t} \\ u_{s,t}^{AG} P_s^{AG,\min} \le P_{s,t}^{AG} \le u_{s,t}^{AG} P_s^{AG,\max} \end{cases} \tag{4.4}$$

$$P_{s,t}^{AES,L} = \sum_{b\in\mathcal{B}} X_{b,s,t} P_s^{SL} \tag{4.5}$$

The constraints of onboard ESSs include

$$\begin{cases} E_{s,t}^{AES} = E_{s,t-1}^{AES} + \eta_s^{AES,ch} P_{s,t}^{AES,ch} - \dfrac{P_{s,t}^{AES,dis}}{\eta_s^{AES,dis}} \\ E_s^{AES,\min} \le E_{s,t}^{AES} \le E_s^{AES,\max} \\ E_{s,T}^{AES} = E_s^{AES,Req} \end{cases} \tag{4.6}$$

where the third line ensures that required energy level should be reached when the AES departs. Note that $SOC_{s,T}^{AES} = SOC_{s,t_s^d}^{AES}$ due to constraint (4.3).

The power demand of AES on node j is denoted as:

$$P_{j,t}^{SPDN,AES} = \sum_{b\in\Pi(j)} \sum_{s\in\mathcal{S}} X_{b,s,t} \left(P_{s,t}^{G2S} - P_{s,t}^{S2G}\right) \tag{4.7}$$

where $\Pi(j)$ represent the set of berths connected to the node j of SPDN. The equation's right side is the product of binary variable and continuous variable, which can be linearized by big-M method. With equation (4.7), we can see that the flexibility from AES is significantly enhanced by dual demand response from both the adjustment of berthing status $X_{b,s,t}$ and net power demand $P_{s,t}^{G2S} - P_{s,t}^{S2G}$, along with potential energy feedback.

2) Modeling of QC: Similar to AES, the operational status of QC is denoted by a three-dimensional binary variable $\omega_{q,s,t}$, which equals to 1 when QC q serves AES s at time t, otherwise, it is 0. The QC assignment constraints include:

$$\sum_{s\in\mathcal{S}} \omega_{q,s,t} \le 1 \tag{5.1}$$

$$\sum_{q\in\mathcal{Q}} \sum_{s\in\mathcal{S}} \omega_{q,s,t} \le Q^{\max} \tag{5.2}$$

$$Q_s^{\min} \sum_{b\in\mathcal{B}} X_{b,s,t} \le \sum_{q\in\mathcal{Q}} \omega_{q,s,t} \le Q_s^{\max} \sum_{b\in\mathcal{B}} X_{b,s,t} \tag{5.3}$$

$$\sum_{q\in\mathcal{Q}} \sum_{t\in\mathcal{T}} \omega_{q,s,t} \eta_{q,t}^{QC} = TEU_s^{Req} \tag{5.4}$$

Constraint (5.1) ensures that each QC can serve at most one AES at any time. Constraint (5.2) limits the total number of available QCs. Constraint (5.3) restricts the number of assigned QCs for AES. Constraint (5.4) indicates that the cargo handling task should be completed before AES departs.

The power load of QC in the literature is formulated similarly to AES, expressed as $\sum_{s\in\mathcal{S}} \omega_{q,s,t} P_q^{QC}$, where P_q^{QC} represents the constant power demand of QC for lifting up cargoes. The demand response can only be achieved by adjusting QC status $\omega_{q,s,t}$. However, this modeling approach neglects the energy conversion process of QC and its energy feedback capacity when equipped with ESS. Specifically, Fig. 2 depicts the power profile of the motor in QC during one cargo handling cycle. The motor serves as an electric load when lifting up and as a generator when lifting down due to gravitational potential energy conversion. The regenerated braking energy during the lifting down phase can be stored in embedded ESS or fed back to SPDN. In this sense, the power demand of QC is not only the power required for lifting up, but the comprehensive result of lifting up, lifting down (energy recovery), and the charging/discharging of ESS. Given that, the energy balance condition of QC

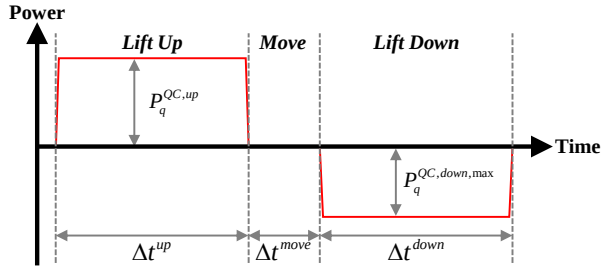

Fig. 2. Power profile of motor in QC in one cargo handling cycle.

electric drive system in one cargo handling cycle is expressed as:

$$\begin{cases} \left(P_{q,t}^{G2Q} - P_{q,t}^{Q2G}\right)\Delta t_q + P_{q,t}^{QC,dis}\Delta t_q = P_{q,t}^{QC,ch}\Delta t_q \\ \qquad + \left(P_q^{QC,up}\Delta t_q^{up} - P_{q,t}^{QC,down}\Delta t_q^{down}\right) \\ 0 \le P_{q,t}^{QC,down} \le P_q^{QC,down,\max} \end{cases} \tag{6.1}$$

where $\Delta t_q = \Delta t_q^{up} + \Delta t_q^{move} + \Delta t_q^{down}$ represents the total time consumption of one cargo handling cycle. The power exchange between QC and SPDN is represented by $P_{q,t}^{G2Q} - P_{q,t}^{Q2G}$, which is positive when SPDN delivers power to QC, otherwise, QC feeds energy back to SPDN.

To unify the time-scale of QC with other logistic components and SPDN, (6.1) is expanded from one cycle to 1 hour resolution as:

$$\begin{cases} \left(P_{q,t}^{G2Q} - P_{q,t}^{Q2G}\right) + P_{q,t}^{QC,dis} = P_{q,t}^{QC,ch} \\ \qquad + \eta_{q,t}^{QC} P_q^{QC,up}\Delta t_q^{up} - \sum_{n^{QC}=1}^{\eta_{q,t}^{QC}} P_{q,t,n^{QC}}^{QC,down}\Delta t_q^{down} \\ 0 \le P_{q,t,n^{QC}}^{QC,down} \le P_q^{QC,down,\max} \end{cases} \tag{6.2}$$

where $P_{q,t,n^{QC}}^{QC,down}$ is the utilized regenerated power in cycle n^{QC} at time t. Considering that the cargo handling efficiency $\eta_{q,t}^{QC}$ means the number of cycles in 1 hour, $\eta_{q,t}^{QC} P_q^{QC,up}\Delta t_q^{up}$ is hourly power demand for lifting up, and $\sum_{n^{QC}=1}^{\eta_{q,t}^{QC}} P_{q,t,n^{QC}}^{QC,down}\Delta t_q^{down}$ is hourly utilized regenerated energy. The term $\sum_{n^{QC}=1}^{\eta_{q,t}^{QC}} P_{q,t,n^{QC}}^{QC,down}\Delta t_q^{down}$ is nonlinear due to the decision variable $\eta_{q,t}^{QC}$. To tackle this, a new variable $\hat{P}_{q,t}^{QC,down}$ is introduced to equivalently replace it. Since $P_q^{QC,up}$ and $P_q^{QC,down,\max}$ exist only when the QC is working, the final linear version of power balance equation for 1 hour resolution is formulated as follows:

$$\begin{cases} \left(P_{q,t}^{G2Q} - P_{q,t}^{Q2G}\right) + P_{q,t}^{QC,dis} = P_{q,t}^{QC,ch} \\ \qquad + \eta_{q,t}^{QC}\sum_{s\in\mathcal{S}} \omega_{q,s,t} P_q^{QC,up}\Delta t_q^{up} - \hat{P}_{q,t}^{QC,down}\Delta t_q^{down} \\ 0 \le \hat{P}_{q,t}^{QC,down} \le \eta_{q,t}^{QC}\sum_{s\in\mathcal{S}} \omega_{q,s,t} P_q^{QC,down,\max} \end{cases} \tag{7.1}$$

Differing from AES, the embedded ESS in QC is allowed to charge/discharge regardless of whether QC is working or not, providing more flexibility for SPDN. The constraints of ESS are stated as below:

$$\begin{cases} P_{q,t}^{QC,ch/dis,\min} \le P_{q,t}^{QC,ch/dis} \le P_{q,t}^{QC,ch/dis,\max} \\ E_{q,t}^{QC} = E_{q,t-1}^{QC} + \eta_q^{QC,ch} P_{q,t}^{QC,ch} - \dfrac{P_{q,t}^{QC,dis}}{\eta_q^{QC,dis}} \\ E_q^{QC,\min} \le E_{q,t}^{QC} \le E_q^{QC,\max} \end{cases} \tag{7.2}$$

The power demand of QC on node j is expressed as:

$$P_{j,t}^{SPDN,QC} = \sum_{q\in\Phi(j)} \left(P_{q,t}^{G2Q} - P_{q,t}^{Q2G}\right) \tag{7.3}$$

where $\Phi(j)$ represent the set of QCs connecting to the node j of SPDN. Equation (7.3) indicates that QC at any operational status can exchange power with SPDN, and offer significant flexibility through status adjustment, variable net power demand and energy feedback.

3) Modeling of AGV and BSS: In battery charging mode, AGV and battery are modeled as a whole. Different from that, in battery swapping mode, we treat AGV and battery as two independent entities. To account for the location of battery (either on AGV or in the BSS), two binary variables $I_{n,v,t}^{onAGV}$ and $I_{n,t}^{onBSS}$ are introduced. They equal to 1 if battery n is on AGV v or in the BSS at time t. The AGV has three statuses: working, denoted by $\sigma_{v,q,t}^{work}$, swapping battery, denoted by $\sigma_{v,q,t}^{swap}$, and idle, denoted by $\sigma_{v,t}^{idle}$. Specifically, $\sigma_{v,q,t}^{work}$ is 1 if AGV v is serving QC q at time t, $\sigma_{v,q,t}^{swap}$ is 1 if AGV v first swaps new battery from BSS and then serves QC q at time t, and $\sigma_{v,t}^{idle}$ is 1 if AGV v is idle at time t. Additionally, four binary variables $\delta_{n,v,t}^{work}$, $\delta_{n,v,t}^{swapin}$, $\delta_{n,v,t}^{swapout}$, $\delta_{n,v,t}^{idle}$ are introduced to match each AGV with one battery. $\delta_{n,v,t}^{work}/\delta_{n,v,t}^{idle}$ is 1 if AGV v equipped with battery n is working/idle at time t, and $\delta_{n,v,t}^{swapin}/\delta_{n,v,t}^{swapout}$ is 1 if battery n is put into/removed from AGV v at time t. With these variables, the battery swapping constraints are formulated as:

$$\sum_{n\in\mathcal{N}} I_{n,v,t}^{onAGV} = 1 \tag{8.1}$$

$$I_{n,t}^{onBSS} + \sum_{v\in\mathcal{V}} I_{n,v,t}^{onAGV} = 1 \tag{8.2}$$

$$\delta_{n,v,t}^{idle} + \delta_{n,v,t}^{swapin} + \delta_{n,v,t}^{work} = I_{n,v,t}^{onAGV} \tag{8.3}$$

$$\sigma_{v,t}^{idle} + \sum_{q\in\mathcal{Q}} \sigma_{v,q,t}^{swap} + \sum_{q\in\mathcal{Q}} \sigma_{v,q,t}^{work} = 1 \tag{8.4}$$

$$\begin{cases} I_{n,v,t}^{onAGV} - I_{n,v,t-1}^{onAGV} = \delta_{n,v,t}^{swapin} - \delta_{n,v,t}^{swapout} \\ I_{n,v,t}^{onAGV} \ge \delta_{n,v,t}^{swapin} \\ 1 - I_{n,v,t}^{onAGV} \ge \delta_{n,v,t}^{swapout} \end{cases} \tag{8.5}$$

$$\begin{cases} \sum_{n\in\mathcal{N}} \delta_{n,v,t}^{idle} = \sigma_{v,t}^{idle} \\ \sum_{n\in\mathcal{N}} \left(\delta_{n,v,t}^{swapin} + \delta_{n,v,t}^{swapout}\right) = 2\sum_{q\in\mathcal{Q}} \sigma_{v,q,t}^{swap} \\ \sum_{n\in\mathcal{N}} \delta_{n,v,t}^{work} = \sum_{q\in\mathcal{Q}} \sigma_{v,q,t}^{work} \end{cases} \tag{8.6}$$

$$\begin{cases} \eta_{q,t}^{QC} = \sum_{v\in\mathcal{V}} \left(\eta_{v,q,t}^{AGV,swap} + \eta_{v,q,t}^{AGV,work}\right) \\ 0 \le \eta_{q,t}^{QC} \le \eta_q^{QC,\max} \\ 0 \le \eta_{v,q,t}^{AGV,swap} \le \sigma_{v,q,t}^{swap}\eta_v^{AGV,swap,\max} \\ 0 \le \eta_{v,q,t}^{AGV,work} \le \sigma_{v,q,t}^{work}\eta_v^{AGV,work,\max} \end{cases} \tag{8.7}$$

$$\begin{cases} \sigma_{v,q,t}^{swap} \le \sum_{s\in\mathcal{S}} \omega_{q,s,t} \\ \sigma_{v,q,t}^{work} \le \sum_{s\in\mathcal{S}} \omega_{q,s,t} \end{cases} \tag{8.8}$$

$$\begin{aligned} &\left(I_{n,t}^{onBSS} - \sum_{v\in\mathcal{V}} \delta_{n,v,t}^{swapout}\right) P_{n,t}^{BT,ch/dis,\min} \\ &\quad + \alpha^{swap} \sum_{v\in\mathcal{V}} \delta_{n,v,t}^{swapout} P_{n,t}^{BT,ch/dis,\min} \le P_{n,t}^{BT,ch/dis} \\ &\quad \le \left(I_{n,t}^{onBSS} - \sum_{v\in\mathcal{V}} \delta_{n,v,t}^{swapout}\right) P_{n,t}^{BT,ch/dis,\max} \\ &\quad + \alpha^{swap} \sum_{v\in\mathcal{V}} \delta_{n,v,t}^{swapout} P_{n,t}^{BT,ch/dis,\max} \end{aligned} \tag{8.9}$$

$$\begin{cases} E_{n,t}^{BT} = E_{n,t-1}^{BT} + \eta_n^{BT,ch} P_{n,t}^{BT,ch} - \dfrac{P_{n,t}^{BT,dis}}{\eta_n^{BT,dis}} \\ \quad - \sum_{v\in\mathcal{V}} \Delta E_v^{AGV} \left(\begin{array}{l} \delta_{n,v,t}^{swapin} \sum_{q\in\mathcal{Q}} \eta_{v,q,t}^{AGV,swap} \\ + \delta_{n,v,t}^{work} \sum_{q\in\mathcal{Q}} \eta_{v,q,t}^{AGV,work} \end{array} \right) \\ E_n^{BT,\min} \le E_{n,t}^{BT} \le E_n^{BT,\max} \end{cases} \tag{8.10}$$

$$\begin{cases} E_{n,t}^{BT} - \underline{E}_n^{BT,swapin} \ge -M\left(1 - \delta_{n,v,t}^{swapin}\right) \\ \overline{E}_n^{BT,swapout} - E_{n,t}^{BT} \ge -M\left(1 - \delta_{n,v,t}^{swapout}\right) \end{cases} \tag{8.11}$$

Constraint (8.1) ensures that each AGV is equipped with only one battery. Constraints (8.2)-(8.4) restrict the AGV to be in one status at any time. Constraint (8.5) links the swap-in and swap-out actions with the variable $I_{n,v,t}^{onAGV}$. Constraint (8.6) bridges variables δ and σ. Constraint (8.7) calculates the cargo handling efficiency of QC based on AGV transportation efficiency. Constraint (8.8) ensures that the AGV only serves the working QC. As the battery cannot be charged/discharged during swapping process, constraint (8.9) limits charging/discharging power based on AGV status. Here, α^{swap} is a coefficient between 0 and 1, used to account for the time loss caused by battery swapping. Constraint (8.10) calculates battery energy level, where the bilinear terms $\delta_{n,v,t}^{swapin}\eta_{v,q,t}^{AGV,swap}$ and $\delta_{n,v,t}^{work}\eta_{v,q,t}^{AGV,work}$ are linearized by big-M method. Constraint (8.11) restricts that the battery can be put into/removed from the AGV only when the energy level is greater/less than a certain threshold.

The power demand of batteries in the BSS on node j is :

$$P_{j,t}^{SPDN,BSS} = \sum_{n\in\Gamma(j)} \left(P_{n,t}^{BT,ch} - P_{n,t}^{BT,dis}\right) \tag{8.12}$$

where $\Gamma(j)$ is the set of batteries belonging to the BSS connected to the node j of SPDN.

With the above equations, we can see that the battery swap mode offers greater flexibility than the battery charging mode. Since the battery and the AGV are considered separate, the idle batteries in the BSS can be charged at optimal time periods according to the operational status of SPDN without impacting AGV logistics scheduling. In contrast, in battery charging mode, the battery is tethered to the AGV, leading to a coupling of the battery charging time with AGV logistics scheduling. This compulsory linkage may exert additional pressure on SPDN. Furthermore, in battery swapping mode, the idle batteries in the BSS can discharge to support SPDN operation. Conversely, in battery charging mode, AGVs typically do not discharge to SPDN because they needs to be fully charged as quickly as possible and then return to logistics scheduling.

4) Modeling of SPDN: Linear Distflow model is adopted to formulate SPDN as:

$$P_{ij,t}^{line} + \sum_{m\in\Xi(j)} P_{m,t}^{RES} = \sum_{k\in\Theta(j)} P_{jk,t}^{line} + P_{j,t}^{L} \tag{9.1}$$

$$Q_{ij,t}^{line} = \sum_{k\in\Theta(j)} Q_{jk,t}^{line} + Q_{j,t}^{load} \tag{9.2}$$

$$P_{j,t}^{L} = P_{j,t}^{load} + P_{j,t}^{SPDN,AES} + P_{j,t}^{SPDN,QC} + P_{j,t}^{SPDN,BSS} \tag{9.3}$$

$$0 \le P_{m,t}^{RES} \le \left(1 + \xi_{m,t}\right) P_{m,t}^{RES,f} \tag{9.4}$$

$$U_{i,t} - U_{j,t} = r_{ij} P_{ij,t}^{line} + x_{ij} Q_{ij,t}^{line} \tag{9.5}$$

$$U_j^{\min} \le U_{j,t} \le U_j^{\max} \tag{9.6}$$

$$-S_{ij}^{\max} \le P_{ij,t}^{line}, Q_{ij,t}^{line} \le S_{ij}^{\max} \tag{9.7}$$

$$-\sqrt{2}S_{ij}^{\max} \le P_{ij,t}^{line} \pm Q_{ij,t}^{line} \le \sqrt{2}S_{ij}^{\max} \tag{9.8}$$

Constraints (9.1)-(9.2) present power balance equations where $P_{ij,t}^{line} = P_t^{grid,DA} + P_t^{grid,ID,+} - P_t^{grid,ID,-}$ and $Q_{ij,t}^{line} = Q_t^{grid}$ if node j is a substation. Constraints (9.3)-(9.4) calculate nodal power load and available renewable energy. Constraints (9.5)-(9.6) restrict nodal voltage balance and magnitude. Constraints (9.7)-(9.8) provide a linear form of $\left(P_{ij,t}^{line}\right)^2 + \left(Q_{ij,t}^{line}\right)^2 \le \left(S_{ij}^{\max}\right)^2$ [26].

5) Logistic-Energy Collaborative Dispatch Model: With above constraints, the logistic-energy collaborative dispatch model is expressed as a multi-objective optimization problem:

$$\begin{aligned} &\min \ \{f_1, f_2\} + \left\{\sum_{t\in\mathcal{T}} g_{1,t}, \sum_{t\in\mathcal{T}} g_{2,t}\right\} \\ &\text{s.t. } (2), (3), (4), (5), (7), (8), (9) \end{aligned} \tag{10.1}$$

$$\begin{aligned} g_{2,t} = {} & \beta_{s,2}^{AES}\left(P_{s,t}^{AG}\right)^2 + \beta_{s,1}^{AES} P_{s,t}^{AG} + \beta_{s,0}^{AES} u_{s,t}^{AG} + c_t^{grid,ID,+} P_t^{grid,ID,+} + c_t^{grid,ID,-} P_t^{grid,ID,-} \\ & + \sum_{s\in\mathcal{S}} d_s^{AES}\left(P_{s,t}^{AES,ch} + P_{s,t}^{AES,dis}\right) + \sum_{q\in\mathcal{Q}} d_q^{QC}\left(P_{q,t}^{QC,ch} + P_{q,t}^{QC,dis}\right) \\ & + \sum_{n\in\mathcal{N}} d_n^{BT}\left[P_{n,t}^{BT,ch} + P_{n,t}^{BT,dis} + \eta_n^{BT,dis} \sum_{v\in\mathcal{V}} \Delta E_v^{AGV}\left(\delta_{n,v,t}^{swapin} \sum_{q\in\mathcal{Q}} \eta_{v,q,t}^{AGV,swap} + \delta_{n,v,t}^{work} \sum_{q\in\mathcal{Q}} \eta_{v,q,t}^{AGV,work}\right)\right] \end{aligned} \tag{10.4}$$

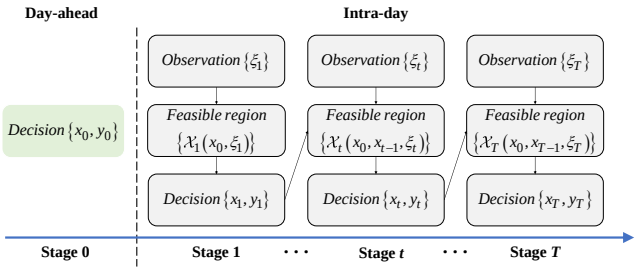

Fig. 3. Dynamic decision-making process of MMDRO.

where

$$\begin{cases} f_1 = \sum_{s\in\mathcal{S}} t_s^d \\ f_2 = \sum_{t\in\mathcal{T}} c_t^{grid,DA} P_t^{grid,DA} \end{cases} \tag{10.2}$$

$$g_{1,t} = \sum_{j\in\mathcal{J}} |U_1 - U_{j,t}| \tag{10.3}$$

f_1 and f_2 are day-ahead optimization objectives aiming to minimize AES departure time (i.e., maximize logistic transportation efficiency) and electricity purchase cost, $\sum_{t\in\mathcal{T}} g_{1,t}$ and $\sum_{t\in\mathcal{T}} g_{2,t}$ are intra-day optimization objectives to minimize the total nodal voltage deviation and the dispatch costs (including electricity adjustment, AES generation and ESS/battery degradation costs). Note that the coefficients $\beta_{s,0/1/2}^{AES}$ integrate power generation cost and carbon emission cost together, which can effectively strike a trade-off between system optimal operation and carbon emissions.

III. Multi-objective Multistage Distributionally Robust Optimization Formulation

In this section, the deterministic logistic-energy collaborative dispatch model (10) is incorporated into the MMDRO framework, to address the renewable energy uncertainties in the system.

A. Scheduling Framework

The MMDRO adopts a dynamic decision-making process as shown in Fig. 3. The day-ahead stage determines AES berth allocation and electricity purchase from the upstream grid. The intra-day problem is formulated as a sequential decision-making process with T stages. At each stage, the optimal decisions, including logistic scheduling of QC and AGV, and energy dispatch of AES, QC, AGV, BSS, and SPDN, are dynamically determined based on sequentially observed uncertainties. Specifically, with the day-ahead decision $\{x_0, y_0\}$, we make the intra-day decision $\{x_1, y_1\}$ when uncertainty ξ_1 is observed at stage 1. The decision x_1 affects the feasible region of $\{x_2, y_2\}$ through time coupling constraints. With that and observed uncertainty ξ_2, the decision $\{x_2, y_2\}$ are made at stage 2. This a dynamic decision-making process continues until reaching stage T. By considering such a dynamic process, the dispatch solutions can effectively ensure non-anticipativity.

B. MMDRO Model

Before formulating MMDRO, equation (5.4) is replaced by the following constraint to ensure that only two adjacent time periods are connected, rather than multiple periods.

$$\begin{cases} TEU_{s,t} = TEU_{s,t-1} + \sum_{q\in\mathcal{Q}} \omega_{q,s,t} \eta_{q,t}^{QC} \\ TEU_{s,t} \le TEU_s^{Req} \\ TEU_{s,T} = TEU_s^{Req} - TEU_s^{penalty} \end{cases}$$

where the penalty term $TEU_s^{penalty}$ is introduced to ensure the feasibility of the problem. Similarly, the third line of equation (4.6) is modified as $E_{s,T}^{AES} = E_s^{AES,Req} - E_s^{AES,penalty}$. Both $TEU_s^{penalty}$ and $E_s^{AES,penalty}$ are added into the objective function $g_{1,T}$ and $g_{2,T}$ by multiplying them with the corresponding penalty coefficients.

The MMDRO model minimizes multiple objectives under the worst-case probability distribution within the ambiguity set. Considering the dynamic decision-making process stated in Fig. 3, the MMDRO model is formulated in a nested structure as follows:

$$\begin{aligned} &\min_{(x_0,y_0)\in\mathcal{X}_0} \Big\{ F(\lambda, x_0, y_0) + \sup_{\mathbb{P}_1\in\mathcal{P}_1} \mathbb{E}_{\mathbb{P}_1} \Big[\min_{(x_1,y_1)\in\mathcal{X}_1(x_0;\xi_1)} G_1(\lambda, x_1, y_1) \\ &+ \sup_{\mathbb{P}_t\in\mathcal{P}_t} \mathbb{E}_{\mathbb{P}_t} \Big[\min_{(x_t,y_t)\in\mathcal{X}_t(x_0,x_{t-1};\xi_t)} G_t(\lambda, x_t, y_t) + \cdots \\ &+ \sup_{\mathbb{P}_T\in\mathcal{P}_T} \mathbb{E}_{\mathbb{P}_T} \min_{(x_T,y_T)\in\mathcal{X}_T(x_0,x_{T-1};\xi_T)} G_T(\lambda, x_T, y_T) \Big] \Big] \Big] \Big\} \end{aligned} \tag{11.1}$$

where

$$\begin{cases} x_0 = \left\{ X_{b,s,t}, P_t^{grid,DA} \right\}, y_0 = \left\{ t_s^b, t_s^d, B_s \right\} \\ x_t = \left\{ E_{s,t}^{AES}, TEU_{s,t}, E_{q,t}^{QC}, I_{n,v,t}^{onAGV}, E_{n,t}^{BT} \right\} \\ y_t = \begin{Bmatrix} P_{s,t}^{G2B/B2G}, \mu_{s,t}^{AG}, P_{s,t}^{AG}, P_{s,t}^{AES,ch/dis}, \omega_{q,s,t}, \eta_{q,t}^{QC} \\ P_{q,t}^{G2Q/Q2G}, P_{q,t}^{QC,ch/dis}, \hat{P}_{q,t}^{QC,down}, I_{n,t}^{onBSS} \\ \sigma_{v,t}^{idle}, \sigma_{v,q,t}^{work/swap}, P_{n,t}^{BT,ch/dis}, \eta_{v,q,t}^{AGV,work/swap} \\ \delta_{n,v,t}^{idle/work/swapin/swapout}, P_{ij,t}^{line}, Q_{ij,t}^{line}, \\ P_t^{grid,ID,+/-}, Q_t^{grid}, U_{j,t}, P_{m,t}^{RES} \end{Bmatrix} \end{cases} \tag{11.2}$$

$$F(\lambda, x_0, y_0) = \lambda f_1 + (1-\lambda) f_2 \tag{11.3}$$

$$G_t(\lambda, x_t, y_t) = \lambda g_{1,t} + (1-\lambda) g_{2,t} \tag{11.4}$$

$$\mathcal{P}_t = \left\{ \mathbb{P}_t \middle| \begin{array}{l} \Pr(\xi_t \in \Omega_t) = 1 \\ \mathbb{E}_{\mathbb{P}}(\xi_t) = \mu_t \\ \mathbb{E}_{\mathbb{P}}\left[(\xi_t - \mu_t)(\xi_t - \mu_t)^T \right] = \Sigma_t \end{array} \right. \tag{11.5}$$

Equation (11.1) presents the objective function of MMDRO, where the uncertainty ξ_t follows the probability measure $\mathbb{P}_t$ taken from the moment-based ambiguity set $\mathcal{P}_t$ (11.5). In (11.2), x_0 and x_t denote state variables that connects different stages, while y_0 and y_t are stage variables that only appear at the corresponding stages. $\mathcal{X}_0$ and $\mathcal{X}_t$ represent the feasible region of $\{x_0, y_0\}$ and $\{x_t, y_t\}$, where $\mathcal{X}_0$ corresponds to constraints (2)-(3), $\mathcal{X}_t$ corresponds to constraints (4)-(5), (7)-(9). Equation (11.3) and (11.4) present the day-ahead and intra-day optimization objectives respectively. Here, $\lambda \in [0, 1]$ is the weight coefficient used to trade off multiple objectives, and its calculation will

This article has been accepted for publication in IEEE Transactions on Transportation Electrification. This is the author's version which has not been fully edited and content may change prior to final publication. Citation information: DOI 10.1109/TTE.2024.3394675

be discussed in Section IV-C. With that, seaport operators can make a balance between optimal economics ($\lambda = 0$) and system operational security-based maximum logistic efficiency ($\lambda = 1$).

IV. Solution Approach For MMDRO Model

The MMDRO model is computationally intractable owing to multiple objectives, nested min-max-min optimization structure, and mixed integer property. In this section, the MMDRO model is first reformulated into a tractable dynamic programming form. Then, an improved multi-objective SDDiP algorithm is developed to efficiently solve it.

A. Dynamic Programming Form

In (11), the feasible region $\mathcal{X}_t$ depends on not only the previous stage's state variable x_{t-1}, but also the day-ahead decision x_0 which spans several stages. To make (11) relies only on previous stage's state variables, dummy state variables s_t and the following constraints are added into the feasible region $\mathcal{X}_t$ to replicate the day-ahead decision x_0.

$$s_t = \begin{cases} x_0, \text{ if } t = 1 \\ L_t s_{t-1}, \text{ if } t \geq 2 \end{cases} \tag{12}$$

where L_t is the matrix that selects certain part of s_t. That means $L_t s_{t-1}$ denotes $\{X_{b,s,t}, ..., X_{b,s,T}\}$ if s_{t-1} represents $\{X_{b,s,t-1}, ..., X_{b,s,T}\}$.

Since a portion of x_0 and x_t are continuous variables while SDDiP algorithm requires all state variables to be binary, binary expansion [30] is employed to convert continuous variables into binary form. For ease of notion, we still use symbol x_0 and x_t to represent their binary form. Then, by adding s_t into x_t, the equivalent recursion of (11.1) is defined by the following value function which depends only on the previous stage's state variables.

$$Q_0(\lambda) = \min_{(x_0, y_0) \in \mathcal{X}_0} F(\lambda, x_0, y_0) + Q_1(\lambda, x_0) \tag{13.1}$$

$$Q_t(\lambda, x_{t-1}; \xi_t) = \min_{(x_t, y_t) \in \mathcal{X}_t(x_{t-1}; \xi_t)} G_t(\lambda, x_t, y_t) + Q_{t+1}(\lambda, x_t) \tag{13.2}$$

where $Q_1(\lambda, x_0)$ and $Q_{t+1}(\lambda, x_t)$ are called the worst-case cost-to-go functions which are defined in (14). Particularly, we have $Q_{T+1}(\lambda, x_T) \equiv 0$.

$$Q_t(\lambda, x_{t-1}) = \max_{p_{r,t} \in \mathcal{P}_t} \sum_{r=1}^{N_t^\xi} p_{r,t} Q_t(\lambda, x_{t-1}; \xi_{r,t}) \tag{14}$$

where the continuous uncertainty value ξ_t in (11.5) is discretized as N_t^ξ realizations, $p_{r,t}$ is the probability distribution corresponding to the realization $\xi_{r,t}$. Note that this paper focuses on the renewable energy uncertainty due to the significantly increasing penetration of renewable energy in electrified seaports. However, the proposed MMDRO framework can easily incorporate power load uncertainty by adding it into $\xi_{r,t}$.

The model (13) is challenging to solve directly due to the implicit value function $Q_{t+1}(\lambda, x_t)$. Typically, the SDDiP algorithm is adopted to approximate the value function by iteratively constructing its under-approximation. However, the UB in standard SDDiP is calculated by the sum of objective values of all stages from all sampling paths. Due to random sampling, UB is volatile and it is difficult to determine in which iteration the solution obtained is truly optimal. To address this issue, we develop an improved multi-objective SDDiP algorithm to achieve a controllable and stable convergence process. The improved algorithm calculates UB by defining the over-approximation of value function. When the gap between UB and lower bound (LB) reaches to zero, the algorithm is considered converged. Since UB and LB are crucial for the convergence criterion, in the following, we first introduce how to construct the over-/under-approximation of value function and obtain the necessary parameters. Besides, due to the mixed integer property of our model, the weight update method is [37] is not applicable. To this end, a two-step weight update approach is developed to tackle this issue.

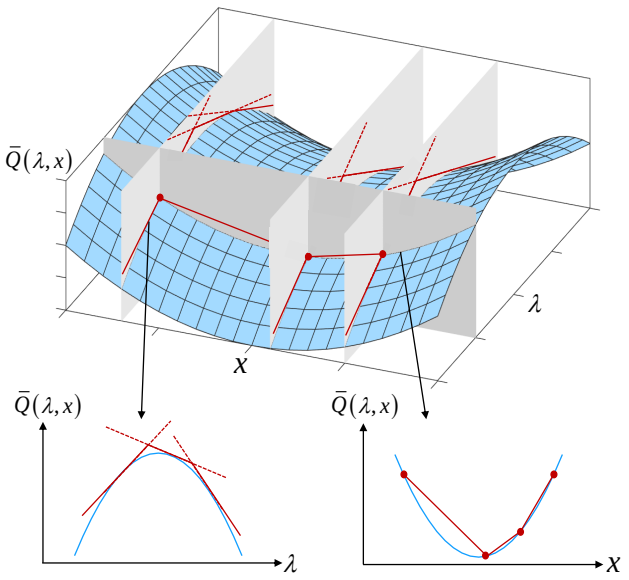

Fig. 4. Illustration of saddle cost-to-go function (blue) and its over-approximation (red).

B. Over-/under-Approximation Construction

In [37], only under-approximation is discussed in detail. Thus, we focus on how to construct the over-approximation of value function in this subsection.

1) Over-Approximation Problem: As Fig. 4 shows, $Q_t(\lambda, x_{t-1})$ is a saddle function which is piecewise-linear convex respect to x_{t-1} and piecewise-linear concave respect to λ. Based on that, the over-approximation problem can be formulated as follows:

$$\begin{aligned} \overline{Q}_t^I(\lambda, x_{t-1}) = \max_{\overline{\mathcal{F}}_t^l} \min_{\gamma_t^l, \gamma_t^+, \gamma_t^-} & \sum_{l=1}^{I-1} \gamma_t^l \overline{\mathcal{F}}_t^l + \overline{L}\left(\gamma_t^+ + \gamma_t^-\right) \\ \text{s.t.} \quad & \overline{\mathcal{F}}_t^l \leq \overline{\theta}_t^l + \frac{\partial \overline{Q}_t^l(\lambda, x_{t-1})}{\partial \lambda}\left(\lambda - \lambda^l\right), \forall l = 1, ..., I-1 \\ & \sum_{i=1}^{I-1} \gamma_t^l = 1 : \varphi_t \\ & x_{t-1} = \sum_{i=1}^{I-1} \gamma_t^l x_{t-1}^l + \gamma_t^+ - \gamma_t^- : \psi_t \\ & \gamma_t^l, \gamma_t^+, \gamma_t^- \geq 0 \end{aligned} \tag{15}$$

where I is the current iteration count, $\overline{L}$ is a large constant, γ_t^+, γ_t^- are slack variables introduced to ensure the problem's feasibility at the beginning of algorithm iteration [32].

The key to constructing (15) are $\overline{\theta}_t^l$ and $\frac{\partial \overline{Q}_t^l(\lambda, x_{t-1})}{\partial \lambda}$, which represent the intercept and slope of supporting hyperplane respect to λ. To obtain them, we first dualize the inner problem of (15) and form the following maximum problem:

$$\begin{aligned} &\overline{Q}_t^I(\lambda, x_{t-1}) = \max_{\varphi_t, \psi_t} \varphi_t + (\psi_t)^T x_{t-1} \\ &\text{s.t. } \varphi_t + (\psi_t)^T x_{t-1}^l \le \overline{\theta}_t^l \\ &\quad + \frac{\partial \overline{Q}_t^l(\lambda, x_{t-1})}{\partial \lambda}\left(\lambda - \lambda^l\right) : \varpi_t^l, \forall l = 1, ..., I-1 \\ &\quad \psi_t \le \overline{L} : \phi_t^+, \quad -\psi_t \le \overline{L} : \phi_t^- \end{aligned} \tag{16}$$

where $\overline{\mathcal{F}}_t^l$ is eliminated by equivalent substitution.

Recall (14), we have

$$\begin{cases} \overline{\theta}_t^I = \sum_{r=1}^{N_t^\xi} p_{r,t}^{I,*} \overline{\theta}_{r,t}^I \\ \dfrac{\partial \overline{Q}_t^I(\lambda, x_{t-1})}{\partial \lambda} = \sum_{r=1}^{N_t^\xi} p_{r,t}^{I,*} \dfrac{\partial \overline{Q}_t^I(\lambda, x_{t-1}; \xi_{r,t})}{\partial \lambda} \end{cases} \tag{17}$$

where $p_{r,t}^{I,*}$ is the worst-case probability distribution obtained at the I^{th} iteration, $\overline{\theta}_{r,t}^I$ is the objective value of the problem:

$$\begin{aligned} &\overline{Q}_t^I(\lambda, x_{t-1}; \xi_{r,t}) \\ &\quad = \min_{(x_t, y_t) \in \mathcal{X}_t} \lambda g_{1,t} + (1-\lambda) g_{2,t} + \overline{Q}_{t+1}^I(\lambda, x_t) \end{aligned} \tag{18}$$

For (18), the decision variables in $\lambda g_{1,t} + (1-\lambda) g_{2,t}$ and $\overline{Q}_{t+1}(\lambda, x_t)$ are independent to each other, thus we further dualize $\overline{Q}_{t+1}(\lambda, x_t)$ and form the problem (19):

$$\begin{aligned} &\overline{Q}_t^I(\lambda, x_{t-1}; \xi_{r,t}) = \\ &\quad \min \lambda g_{1,t} + (1-\lambda) g_{2,t} + \overline{L}^T\left(\phi_{t+1}^+ + \phi_{t+1}^-\right) \\ &\quad + \sum_{l=1}^{I-1} \varpi_{t+1}^l \left(\overline{\theta}_{t+1}^l + \frac{\partial \overline{Q}_{t+1}^l(\lambda, x_t)}{\partial \lambda}\left(\lambda - \lambda^l\right) \right) \\ &\text{s.t. } (x_t, y_t) \in \mathcal{X}_t(x_{t-1}; \xi_{r,t}) \\ &\quad \sum_{l=1}^{I-1} \varpi_{t+1}^l = 1 \\ &\quad x_t = \sum_{l=1}^{I-1} \varpi_{t+1}^l x_t^l + \phi_{t+1}^+ - \phi_{t+1}^- \end{aligned} \tag{19}$$

Since λ only occurs in the objective function, we have

$$\frac{\partial \overline{Q}_t^I(\lambda, x_{t-1}; \xi_{r,t})}{\partial \lambda} = g_{1,t} - g_{2,t} + \sum_{l=1}^{I-1} \varpi_{t+1}^l \frac{\partial \overline{Q}_{t+1}^l(\lambda, x_t)}{\partial \lambda} \tag{20}$$

Based on above analysis, the over-approximation of $Q_t(\lambda, x_{t-1})$ can be constructed in the form of (16), and the parameters can be calculated using (17), (18), (20).

2) Under-Approximation Problem: The under-approximation is formulated in the following form:

$$\begin{aligned} &\underline{Q}_t^I(\lambda, x_{t-1}) = \min_{\kappa_t, \vartheta_t} \kappa_t + \lambda \vartheta_t \\ &\text{s.t. } \kappa_t + \lambda^l \vartheta_t \ge \underline{\theta}_t^l + \left(\rho_t^l\right)^T x_{t-1}, \forall l = 1, ..., I-1 \\ &\quad -\underline{L} \le \vartheta_t \le \underline{L} \end{aligned} \tag{21}$$

Algorithm 1: Improved Multi-objective SDDiP

Initialize: convergence criterion ϵ, $\underline{Q}_t^1 \leftarrow 0$, $\overline{Q}_t^1 \leftarrow +\infty$, $\forall t \in \mathcal{T}$, $\underline{Q}_{T+1}^{\forall I}$, $\overline{Q}_{T+1}^{\forall I} \leftarrow 0$, $LB \leftarrow 0$, $UB \leftarrow +\infty$, $I \leftarrow 1$, $\lambda^1 \leftarrow 1$
while $UB - LB > \epsilon$ **do**
  Solve $\underline{Q}_0\left(\lambda^1\right)$ and save day-ahead decision $\left\{x_0^1, y_0^1\right\}$
  Forward step
  for $t = 1 : T$ **do**
    for $r = 1 : N_t^\xi$ **do**
      Solve $\underline{Q}_t^I\left(\lambda^I, x_{t-1}^I; \xi_{r,t}\right)$; save optimal solution $\left\{x_{r,t}^I, y_{r,t}^I\right\}$, $\underline{Q}_{t+1}^I\left(\lambda^I, x_{r,t}^I\right)$ and objective value as $\underline{Q}_{r,t}^I$
      Calculate $\overline{Q}_{t+1}^I\left(\lambda^I, x_{r,t}^I\right)$ and the gap $\ell_{r,t}^I = \overline{Q}_{t+1}^I\left(\lambda^I, x_{r,t}^I\right) - \underline{Q}_{t+1}^I\left(\lambda^I, x_{r,t}^I\right)$
    end
    Find the optimal $r^* = \arg\max \ell_{r,t}^I$ and set $\left\{x_t^I, y_t^I\right\} = \left\{x_{r^*,t}^I, y_{r^*,t}^I\right\}$
  end
  Backward step
  for $t = T : 1$ **do**
    Solve (14) with $Q_t(\lambda, x_{t-1}; \xi_{r,t})$ replaced by $\underline{Q}_{r,t}^I$, obtain the worst-case probability distribution $p_{r,t}^{I,*}$
    for $r = 1 : N_t^\xi$ **do**
      Solve the Lagrange dual problem of $\underline{Q}_t^I\left(\lambda^I, x_{t-1}^I; \xi_{r,t}\right)$ to save $\underline{\theta}_{r,t}^I$ and $\rho_{r,t}^I$
      Solve $\overline{Q}_{t+1}^I\left(\lambda^I, x_{r,t}^I\right)$, save multiplier ϖ_{t+1}^l and objective value, calculate $\overline{\theta}_{r,t}^I$ and $\frac{\partial \overline{Q}_t^I\left(\lambda, x_{t-1}; \xi_{r,t}\right)}{\partial \lambda}$
    end
    Calculate parameters by (17) and (22) and add new cuts into under-/over-approximation problems
  end
  Weight update and second cut generation
  Set $\lambda^{I+1} \leftarrow 1$ if $\lambda^I = 0$, otherwise, update λ^{I+1} using two-step update method
  Calculate $\underline{Q}_{r,t}^{I+1}$ and implement the Backward step again with λ^{I+1} and $x_{r,t}^I$ to add second cuts
  Update LB and UB by (25); $\lambda^{I+2} \leftarrow \lambda^{I+1}$, $I \leftarrow I+2$
end

where $\underline{\theta}_t^l$ and ρ_t^l are calculated using (22), in which $\underline{\theta}_{r,t}^l$ and $\rho_{r,t}^l$ are obtained by solving the Lagrange dual problem of (23). Further details can be found in [30].

$$\underline{\theta}_t^I = \sum_{r=1}^{N_t^\xi} p_{r,t}^{I,*} \underline{\theta}_{r,t}^I, \quad \rho_t^I = \sum_{r=1}^{N_t^\xi} p_{r,t}^{I,*} \rho_{r,t}^I \tag{22}$$

$$\begin{aligned} &\underline{Q}_t^I(\lambda, x_{t-1}; \xi_{r,t}) \\ &\quad = \min_{(x_t, y_t) \in \mathcal{X}_t} \lambda g_{1,t} + (1-\lambda) g_{2,t} + \underline{Q}_{t+1}^I(\lambda, x_t) \end{aligned} \tag{23}$$

C. Improved Multi-Objective SDDiP Algorithm

The proposed multi-objective SDDiP algorithm with controllable convergence process is presented in Algorithm 1. The algorithm comprises forward and backward steps, two-step weight update and second cut generation.

In the forward step of the standard SDDiP, sampling paths are randomly selected from a scenario tree, and UB is calculated by the sum of objective values of all stages from all sampling paths. Consequently, the UB is volatile and this further affects the judgment on the optimal convergence point.

In contrast, the proposed algorithm traverses all uncertainty realizations at each stage and calculates the gap between the over-approximation and under-approximation for each realization. The optimal solution is selected as the one that achieves the largest gap to help convergence. The UB is calculated by the over-approximation at stage 0, and the iteration stops when the gap between UB and LB converges to zero. Since there is no random sampling, and UB is defined by over-approximation just like LB is defined by under-approximation, the proposed algorithm can converge in a deterministic and controllable way. This reliably helps to find the truly optimal convergence point.

With the solutions obtained from the forward step, the backward step constructs cuts for over-/under-approximation problems. Afterward, λ is updated using the proposed two-step method. In [37], λ is directly updated using the multi-objective simplex method (see Section 6.2 of [40] for details). However, the attribute *reduced cost* does not exist in the mixed-integer MMDRO model. To address this, we propose to calculate λ by the following two steps:

1) Step 1: Select t from 1,…,T and r from 1,…, N_t^{ξ} where the gap is the largest. Solve $\underline{Q}_t\left(\lambda^I, x_{t-1}^I; \xi_{r,t}\right)$ and save the optimal objective value as $\underline{Q}_t^*\left(\lambda^I, x_{t-1}^I; \xi_{r,t}\right)$.

2) Step 2: Relaxing all binary/integer variables of $\underline{Q}_t\left(\lambda^I, x_{t-1}^I; \xi_{r,t}\right)$ into continuous variables, denoted as $\underline{Q}_t^{LP}\left(\lambda^I, x_{t-1}^I; \xi_{r,t}\right)$. Add the following constraint into the LP problem and solve it using multi-objective simplex method to obtain new λ^{I+1}.

$$\begin{aligned}\lambda^I g_{1,t}^{LP} + \left(1-\lambda^I\right) g_{2,t}^{LP} + \underline{Q}_{t+1}^{LP}\left(\lambda^I, x_t^I\right) \\ \geq \underline{Q}_t^*\left(\lambda^I, x_{t-1}^I; \xi_{r,t}\right)\end{aligned} \tag{24}$$

In a word, step 1 is to compute the optimal objective value of the original mixed integer programming (MIP) problem. While in step 2, the objective value of the relaxed LP problem is raised to be at least equal to that of the original MIP problem, ensuring that the LP problem approaches the original problem. Then, with new λ^{I+1} and $x_{r,t}^I$, the backward step is implemented again to construct second cuts for over-/under-approximation problems. Last, LB and UB are updated by performing a sweep along λ for $\underline{Q}_0(\lambda)$ using two-step weight-update method. This leads to a weight sequence $\{\lambda_1, ..., \lambda_M\}$ where $\lambda_1 = 1$, $\lambda_M = 0$, and $\lambda_i > \lambda_{i+1}$. Then, LB and UB are computed as:

$$\begin{cases} LB = \sum_{i=1}^{N-1} \dfrac{\underline{Q}_0(\lambda_i) + \underline{Q}_0(\lambda_{i+1})}{2}(\lambda_i - \lambda_{i+1}) \\ UB = \sum_{i=1}^{N-1} \dfrac{\overline{Q}_0(\lambda_i) + \overline{Q}_0(\lambda_{i+1})}{2}(\lambda_i - \lambda_{i+1}) \end{cases} \tag{25}$$

Remark 1. *(Online Application) After executing Algorithm 1, the well-trained approximation problems with added cuts are obtained. With that, the online application of MMDRO framework can be implemented. Specifically, given a weight coefficient λ, the optimal day-ahead decisions are derived by solving $Q_0(\lambda)$ (13.1) where $Q_1(\lambda, x_0)$ is substituted by its under-approximation (21). Then, the multistage intra-day dispatch is executed period-by-period. That is, after observing the uncertainty realization ξ_t, the optimal decisions at each time period are computed at once by solving $Q_t(\lambda, x_{t-1}; \xi_t)$ (13.2) with $Q_{t+1}(\lambda, x_t)$ replaced by its under-approximation (21). Therefore, we only need to implement Algorithm 1 one time in day-ahead to construct approximation problems, which can be directly used for real-time scheduling without re-calculation.*

Remark 2. *(Convergence and Approximation Error Discussion). The proposed Algorithm 1 can converge in a finite number of iterations, similar to the multi-objective SDDP in [37]. One of the differences between the two algorithms is that our method strategically selects candidate points to construct over-/under-approximation cuts, whereas in the multi-objective SDDP, the candidate points are randomly selected from sampling paths. Although the two algorithms select candidate points in different ways, their iteration process share significant similarities. Considering that the rigorously derived upper-/lower-approximation cuts can form valid and tight bounds for cost-to-go function, the convergence property of Algorithm 1 can be analogous to that of the multi-objective SDDP in [37]. For the approximation errors of cost-to-go function, we claim that the error can be reduced to at least convergence criterion ϵ. This is because the true value of cost-to-go function is sandwiched between the upper and lower approximations. When Algorithm 1 converges, the approximation error is definitely lower than the gap between upper approximation and lower approximation.*

V. Case Studies

A. Basic Settings

In this section, the proposed method is verified via numerical experiments carried out by Python 3.11 and Gurobi 10.0 on a laptop with 13th Gen Intel(R) Core(TM) i9-13900Hz @ 2.60 GHz and 32 GB RAM. The proposed method is validated using the data of Rizhao Port in China. The detailed system data can be found in [41]. The dispatch period T is 24 hours with 1 hour resolution.

B. Comparison Among Different Logistic-Energy Collaborative Dispatch Models

To verify the effectiveness of the proposed logistic-energy collaborative dispatch model, the following four cases are set for comparison:

Case 1: Energy feedback is not considered, the auxiliary generators on AESs are not used, and all ESSs on AESs and QCs are only allowed to be charged and not discharged. The regenerated power of QCs is not utilized, and AGVs operate in battery charging mode.

Case 2: Energy feedback is not considered, and AGVs operate in battery charging mode.

Case 3: Energy feedback is not considered, and AGVs operate in battery swapping mode.

Case 4: The proposed model where energy feedback and AGV battery swapping are both considered.

After solving the above four models using Algorithm 1, the day-ahead decisions and well trained over/under-approximation problems are obtain. With that, a certain scenario of uncertainty realization is given to calculate the intra-day dispatch scheme. Table II presents the simulation results under different weight λ. Fig. 5 and Fig. 6 illustrate the power balance condition and the nodal voltage magnitude.

In terms of logistic transportation efficiency, when $\lambda = 1$, the total departure time of all AESs in Case 3-4 is lower than that in Case 1-2. This highlights that the AGV battery

This article has been accepted for publication in IEEE Transactions on Transportation Electrification. This is the author's version which has not been fully edited and content may change prior to final publication. Citation information: DOI 10.1109/TTE.2024.3394675

TABLE II
COMPARISON BETWEEN CASE 1-4 UNDER DIFFERENT λ

	λ	Case 1	Case 2	Case 3	Case 4
AES departure time (h)	0	93	99	97	101
	0.25	92	96	94	99
	0.5	91	94	93	97
	0.75	88	92	90	94
	1	83	83	81	81
Total dispatch cost ($)	0	131395	120667	119895	90517
	0.25	133029	124025	123029	94872
	0.5	134011	125895	124211	98503
	0.75	134974	127398	125574	100905
	1	136210	131059	129010	102209
Voltage deviation (p.u.)	0	1.330	1.237	1.189	0.823
	0.25	1.325	1.226	1.182	0.820
	0.5	1.322	1.211	1.178	0.809
	0.75	1.316	1.178	1.170	0.797
	1	1.283	1.161	1.083	0.758

swapping mode can achieve higher logistic efficiency than the battery charging mode. As λ decreases, the situation changes. When $\lambda = 0$, the departure time in Case 4 is the largest, while Case 1 has the lowest departure time. This is because Case 4 has the most flexibility resources. To minimize energy cost, AESs are scheduled to delay their departure time to coordinate with SPDN dispatch. In contrast, the flexibility resources in Case 1 are minimal, making delaying AES departure time less beneficial. Despite that, the battery swapping mode maintains its advantage, as with the same energy dispatch condition, the departure time in Case 3 remains lower than that in Case 2 under any value of λ.

In terms of economic performance, as expected, the dispatch cost exhibits a decreasing trend from Case 1 to Case 4. In Case 1, the logistic-side demand response resources only include adjustments to logistic schemes and charging power, leading to lower system flexibility and higher operational costs. In Case 2, although energy feedback is still not allowed, the discharging of ESSs of AESs and QCs, and the utilization of regenerated power of QCs increase the system flexibility, further decreasing operational costs. In Case 3, the dispatch cost further reduces. On one hand, the battery swapping mode shortens the berthing duration of AESs, leading to a reduction in the total power demands of both AESs and QCs throughout the entire dispatch period. On the other hand, the flexible battery swapping mode allows the batteries in the BSS to be charged under the situation of lower electricity price is lower or higher output of renewable energy. Due to these two factors, Case 3 exhibits a lower dispatch cost compared to Case 2. In Case 4, the energy feedback from logistic system provides strong support for SPDN, resulting in less electricity purchase and lower dispatch costs. As depicted in Fig. 5, in Case 1, due to the non-utilization of auxiliary generators on AESs and the restriction on ESSs to only charge without discharging, their power loads are directly supported by the grid-side. Consequently, comparing to Cases 2-3 in Fig. 5(b)-(c), there is more G2S and G2Q power in Case 1. Additionally, in Case 4, the system operations benefit significantly from energy feedback. This leads to more frequent power exchange between SPDN and logistic-side, illustrated by higher G2S/S2G and G2Q/Q2G power in Fig. 5(d).

In terms of voltage regulation, the performance of Case

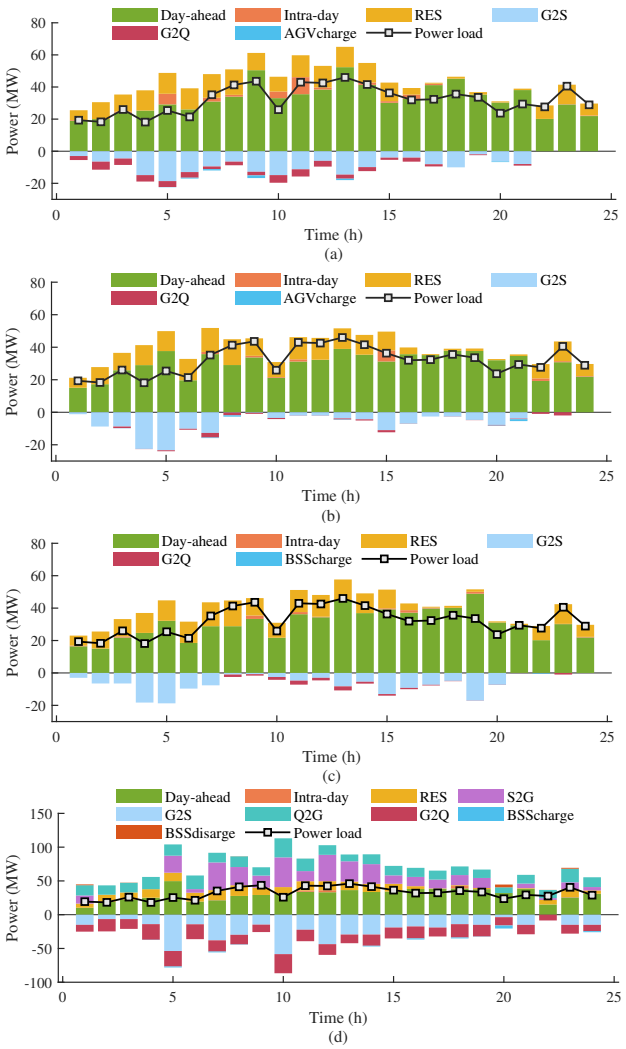

Fig. 5. Power balance condition in SPDN under $\lambda = 0.5$: (a) Case 1; (b) Case 2; (c) Case 3; (d) Case 4.

1-4 is similar to that in economic comparison. As Fig. 6 shows, the average voltage deviation of all nodes in Case 4 is lowest, while Case 1 has the worst performance among the four models. Case2 and Case3 have similar performance, but overall, Case 3 exhibits superior voltage regulation due to more flexible battery swapping mode.

Despite that the voltage deviation in Fig. 6 is not large due to small line resistance and impedance in SPDN, potential voltage violations may occur as the seaport continues to develop. To assess the capability of our method in supporting the SPDN under increased loads, we intentionally raise the conventional power load. Specifically, the voltage constraint (9.6) is relaxed and converted into the penalty term in the objective function. The constant active load level is increased from 150% to 400%, and the test results of minimum voltage magnitude of all nodes across entire dispatch periods are presented in Fig. 7. It is evident that the voltage magnitudes in the four cases decrease as the load level increases. When the load level reaches 250% of its original value, the voltage magnitudes of Cases 1-3 fall below the lower limit (0.95 p.u.). This illustrates that the optimization problem will be infeasible if voltage constraint exists. In contrast, the lower limit is violated in Case 4 only when the load level reaches 400%, illustrating that the proposed method offers strong support for SPDN under high load levels.

This article has been accepted for publication in IEEE Transactions on Transportation Electrification. This is the author's version which has not been fully edited and content may change prior to final publication. Citation information: DOI 10.1109/TTE.2024.3394675

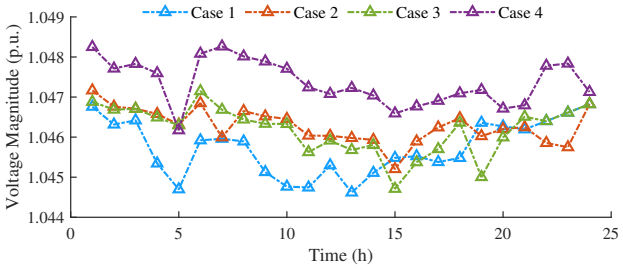

Fig. 6. Average voltage magnitude of all nodes in SPDN under $\lambda = 0.5$.

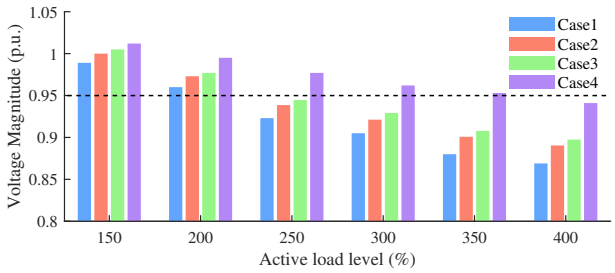

Fig. 7. Minimum voltage magnitude of all nodes across entire dispatch periods.

TABLE III
COMPARISON BETWEEN DIFFERENT UNCERTAINTY HANDLING APPROACHES UNDER $\lambda = 0.5$

	Dispatch cost ($)			AES departure time (h)	Voltage deviation (p.u.)
	Day-ahead	Intra-day	Total		
MMSP	67670	32382	100052	97	0.821
MMRO	70360	31283	101643	98	0.816
MTDRO	68243	32495	100738	96	0.831
MMDRO	68660	29843	98503	97	0.809

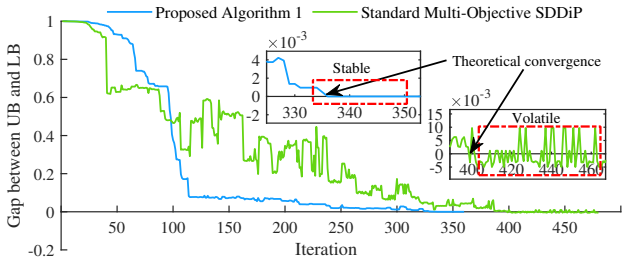

Fig. 8. The gap between UB and LB in Algorithm 1 and standard multi-objective SDDiP.

C. Effect of MMDRO

In this subsection, the proposed MMDRO is compared with multi-objective multistage SP (MMSP), multi-objective multistage RO (MMRO), and multi-objective two-stage DRO (MTDRO) methods. The day-ahead decisions and the cuts for over/under-approximation problems of MMSP, MMRO, and MMDRO are computed by Algorithm 1, where MMSP assumes a known probability distribution, and MMRO allows only one scenario with the probability of 100%. Then, using well-trained under-approximation problems and the given uncertainty realization, T single-period intra-day dispatch problems are solved. For MTDRO, the intra-day dispatch problem is established as only one stage with T time periods, and the model is also solved by Algorithm 1. However, since only day-ahead decisions and cuts for the day-ahead stage can be obtained, the dynamic intra-day decision-making of MTDRO cannot be directly implemented. To address this, a multi-period look-ahead optimization approach is adopted for the intra-day dispatch of MTDRO, which is the state-of-the-art method used in current practice [28].

To test the out-of-sample performance of the four methods, 10,000 scenarios of uncertainty realizations are generated using Monte Carlo Simulation, where the uncertainty variable is assumed to follow a normal distribution with a mean of 0 and a standard deviation of 0.05. The average performance of the four methods under $\lambda = 0.5$ is shown in Table III

The comparison results illustrate that MMDRO achieves the lowest total dispatch cost and voltage deviation among the four methods. Although MMSP exhibits a lower day-ahead dispatch cost, its reliance on precise probability distributions limits its practical performance in intra-day scheduling. MMRO provides solutions under the worst-case scenario, leading to over-conservative decisions and higher costs and voltage deviations. In this regard, MMDRO achieves a satisfactory balance between economics and robustness. For MTDRO and MMDRO, the cuts for under-approximation problems of each intra-day stage of MMDRO are fully adaptive. This implies that the generated cuts construct a complete decision tree for each stage, covering and simulating the decision-making process of subsequent stages. Consequently, the optimal decisions can be made based on real-time observed uncertainty. In contrast, the multi-period look-ahead intra-day dispatch of MTDRO uses forecast renewable output to implement a rolling-horizon optimization. Only the decision of the current stage is adopted, and the time horizon moves forward to the next stage. This method cannot effectively handle uncertainty since the uncertainty in remaining stages is based on forecast values. And the dispatch decisions are not non-anticipative because the current stage decision relies on forecast uncertainty for remaining stages, resulting in sub-optimal decisions. Furthermore, the training method of day-ahead decisions assumes that intra-day dispatch is a single-stage optimization problem with T time periods, which is inconsistent with the actual dispatch method used in intra-day (multi-period look-ahead optimization). Such inconsistency further diminishes the quality and optimality of dispatch solutions, contributing to its inferior performance compared to MMDRO.

D. Algorithm Performance

This subsection compares the proposed Algorithm 1 with standard multi-objective SDDiP. Since there is no record of the standard multi-objective SDDiP in literature, we construct it by combining standard multi-objective SDDP [37] with single-objective SDDiP [30] and two-step weight update method developed in Section IV-C. That means the algorithm procedure inherits that of standard multi-objective SDDP, while the cuts are generated by the approach in single-objective SDDiP, and λ is updated by the two-step method.

Fig. 8 illustrates the convergence process of the gap between UB and LB in the two algorithms. At the beginning of the iteration, the gap in standard multi-objective SDDiP drops sharply, while the gap in Algorithm 1 gradually decreases. This is because the UB in standard multi-objective

This article has been accepted for publication in IEEE Transactions on Transportation Electrification. This is the author's version which has not been fully edited and content may change prior to final publication. Citation information: DOI 10.1109/TTE.2024.3394675

TABLE IV
PROBLEM SCALE SETTING IN THE IEEE 33-BUS SYSTEM

	Scale				
	1	2	3	4	5
Berth	6	10	12	15	15
AES	8	12	15	18	20
QC	12	20	25	28	30
AGV	20	30	35	40	45
Battery	30	40	45	50	55

SDDiP is computed by the sum of objective values of all stages. The large penalty terms at stage T decay rapidly after several valid cuts are added. However, in Algorithm 1, the UB is defined by over-approximation. The slack variables are chosen to be used in the over-approximation problems because the obtained candidate points are not sufficient to cover most of the variable feasible region. This results in a large UB.

In the middle of the iteration, Algorithm 1 exhibits a relatively smooth convergence process, compared to the volatile fluctuations observed in the standard multi-objective SDDiP (this is its typical feature). Such distinction arises from the different definitions of UB in the two algorithms. Additionally, Algorithm 1 illustrates a quicker convergence to the theoretical convergence point compared to standard SDDiP. This is because Algorithm 1 strategically selects the optimal solution for each stage based on the largest gap between over-approximation and under-approximation. This means that the existing cuts corresponding to that solution are the most incomplete (because the gap is large). Thus, the newly added cuts for that solution can construct a relatively complete approximation for the cost-to-go function to the maximum extent, without causing redundancy. In contrast, in the standard multi-objective SDDiP, the obtained solution and generated cuts all rely on randomly selected sample paths. Due to this, the existing cuts at that solution may have been constructed relatively completely, and consequently, the newly generated cuts may be redundant and do not significantly improve LB. This results in the ineffectiveness of the current iteration and reduces the overall convergence speed of the algorithm.

After both algorithms converge, the gap in Algorithm 1 remains constant, whereas the gap in standard multi-objective SDDiP not only increases again but also continues to exhibit volatility. This observation suggests that, despite the algorithm appears to have converged, the attained convergence point may not be genuinely optimal. In this regard, its random and unpredictable convergence behavior poses challenges in determining the optimal iteration count. Furthermore, due to its reliance on random sampling process, the algorithm lacks reproducibility, making it less amenable to real-world engineering applications.

E. Scalability Analysis

This subsection explores the scalability of our proposed method by conducting simulations on a large-scale test system. Because the area of SPDN is typically small, we employ the IEEE-33 bus system as its topology, and focus on the number of logistics equipment. Five problem scales are set in Table IV, where the contents represent the number of Berth/AES/QC/AGV/Battery. Fig. 9 shows the computation time of Algorithm 1 in day-ahead training. As we can see, the computation time gradually increases as the problem scale grows. Nevertheless, it remains within an acceptable range. Given that the computation is completed day-ahead, our algorithm demonstrates good scalability and applicability. Note that the intra-day single period problem can be optimized within seconds using obtained day-ahead decisions and trained under-approximation problems, its calculation time is not presented here. In addition, Fig. 10 compares the dispatch cost and total voltage deviation of Cases 1-4 under different problem scales. As the number of logistics equipment increases, the system needs to support more power loads, resulting in an upward trend of both dispatch cost and voltage deviation. However, it is clearly shown that Case 4 still performs best while Case 1 is the worst, and Cases 2-3 are between them. Overall, the results from the 33-bus system are consistent with those from the Rizhao port system, illustrating the scalability and generality of proposed method.

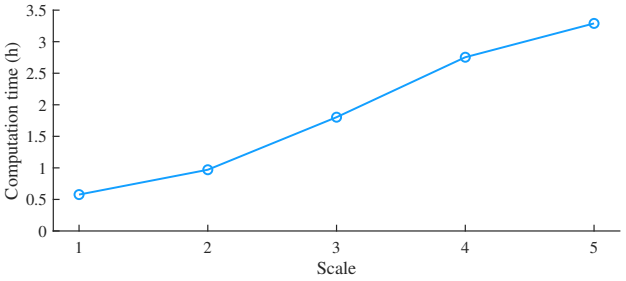

Fig. 9. Computation time of Algorithm 1 under different problem scales.

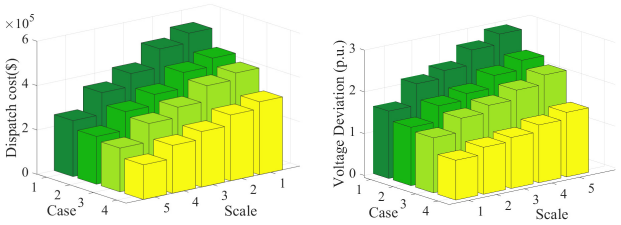

Fig. 10. Dispatch cost and voltage deviation under different problem scales.

VI. CONCLUSION

This paper proposes a flexibility enhancement approach for seaport logistic-energy coordination under renewable energy uncertainty. Firstly, a novel logistic-energy collaborative dispatch model is developed to integrate the energy feedback of AES and QC, as well as the AGV battery swapping mode, into the logistic-energy coordination process. Then, to address uncertainties related to renewable energy in the system, a MMDRO scheduling framework is established to achieve non-anticipative multi-objective dispatch for logistic-energy coordination. An improved multi-objective SDDiP algorithm with a two-stage weight update is then proposed to solve the model in a controllable and stable way.

Numerical simulations are conducted to compare the proposed method with existing methods. The results indicate that energy feedback and AGV battery swapping can significantly increase system flexibility, leading to reduced operational costs and improved voltage deviation. Furthermore, logistic

transportation efficiency is enhanced by the win-win battery swapping mode compared to the battery charging mode. Additionally, MMDRO effectively addresses uncertainties in renewable energy through non-anticipativity dynamic dispatch, resulting in lower objective values compared to multi-objective multistage SP, RO, and two-stage DRO models. Moreover, the improved multi-objective SDDiP algorithm achieves a stable and controllable convergence process compared to the standard multi-objective SDDiP. Lastly, tests on large-scale problems demonstrate the good scalability of the proposed algorithm.

Future work may consider incorporating multiple uncertainties, such as AES arrival time, into multistage scheduling framework for system operation enhancement.

REFERENCES

[1] S. Fang, Y. Wang, B. Gou, and Y. Xu, "Toward future green maritime transportation: An overview of seaport microgrids and all-electric ships," *IEEE Transactions on Vehicular Technology*, vol. 69, no. 1, pp. 207–219, 2020.

[2] G. Sulligoi, D. Bosich, R. Pelaschiar, G. Lipardi, and F. Tosato, "Shore-to-ship power," *Proceedings of the IEEE*, vol. 103, no. 12, pp. 2381–2400, 2015.

[3] Y. Luo, S. Fang, T. Niu, A. Fan, and R. Liao, "Hierarchical power management of shipboard hybrid energy storage system under multiple pulse loads," *IEEE Transactions on Industry Applications*, vol. 60, no. 1, pp. 1380–1395, 2024.

[4] G. Parise, L. Parise, L. Martirano, P. B. Chavdarian, C.-L. Su, and A. Ferrante, "Wise port and business energy management: Port facilities, electrical power distribution," *IEEE Transactions on Industry Applications*, vol. 52, no. 1, pp. 18–24, 2016.

[5] S. G. E. A. Atulya Misra, Gayathri Venkataramani and V. Ramalingam, "Renewable energy based smart microgrids—a pathway to green port development," *Strategic Planning for Energy and the Environment*, vol. 37, no. 2, pp. 17–32, 2017.

[6] Y. Lu, S. Fang, G. Chen, T. Niu, and R. Liao, "Cyber-physical integration for future green seaports: Challenges, state of the art and future prospects," *IEEE Transactions on Industrial Cyber-Physical Systems*, vol. 1, pp. 21–43, 2023.

[7] X. Wang, W. Huang, W. Wei, N. Tai, R. Li, and Y. Huang, "Day-ahead optimal economic dispatching of integrated port energy systems considering hydrogen," *IEEE Transactions on Industry Applications*, vol. 58, no. 2, pp. 2619–2629, 2022.

[8] X. Xiang and C. Liu, "An expanded robust optimisation approach for the berth allocation problem considering uncertain operation time," *Omega*, vol. 103, p. 102444, 2021.

[9] D. Sun, L. Tang, and R. Baldacci, "A benders decomposition-based framework for solving quay crane scheduling problems," *European Journal of Operational Research*, vol. 273, no. 2, pp. 504–515, 2019.

[10] K. H. Kim and J. W. Bae, "A look-ahead dispatching method for automated guided vehicles in automated port container terminals," *Transportation Science*, vol. 38, no. 2, pp. 224–234, 2004.

[11] A. Agra and M. Oliveira, "Mip approaches for the integrated berth allocation and quay crane assignment and scheduling problem," *European Journal of Operational Research*, vol. 264, no. 1, pp. 138–148, 2018.

[12] X. Chen, S. He, Y. Zhang, L. C. Tong, P. Shang, and X. Zhou, "Yard crane and agv scheduling in automated container terminal: A multi-robot task allocation framework," *Transportation Research Part C: Emerging Technologies*, vol. 114, pp. 241–271, 2020.

[13] F. D. Kanellos, E.-S. M. Volanis, and N. D. Hatziargyriou, "Power management method for large ports with multi-agent systems," *IEEE Transactions on Smart Grid*, vol. 10, no. 2, pp. 1259–1268, 2019.

[14] F. D. Kanellos, "Multiagent-system-based operation scheduling of large ports' power systems with emissions limitation," *IEEE Systems Journal*, vol. 13, no. 2, pp. 1831–1840, 2019.

[15] A. Mao, T. Yu, Z. Ding, S. Fang, J. Guo, and Q. Sheng, "Optimal scheduling for seaport integrated energy system considering flexible berth allocation," *Applied Energy*, vol. 308, p. 118386, 2022.

[16] X. Sun, J. Qiu, Y. Tao, Y. Yi, and J. Zhao, "Distributed optimal voltage control and berth allocation of all-electric ships in seaport microgrids," *IEEE Transactions on Smart Grid*, vol. 13, no. 4, pp. 2664–2674, 2022.

[17] Çağatay Iris and J. S. L. Lam, "Optimal energy management and operations planning in seaports with smart grid while harnessing renewable energy under uncertainty," *Omega*, vol. 103, p. 102445, 2021.

[18] Y. Pu, H. Liu, J. Wang, and Y. Hou, "Collaborative scheduling of port integrated energy and container logistics considering electric and hydrogen-powered transport," *IEEE Transactions on Smart Grid*, vol. 14, no. 6, pp. 4345–4359, 2023.

[19] Y. Huang, W. Huang, M. Shahidehpour, N. Tai, C. Li, and R. Li, "Multi-stage dispatch of seaport power systems for incorporating logistical flexibilities in uncertain operational conditions," *IEEE Transactions on Transportation Electrification*, pp. 1–1, 2023.

[20] A. Luque, I. Harrison, S. Pietrosanti, F. M. M. Alasali, W. Holderbaum, R. M. Mayer, and V. M. Becerra, "Energy reduction on ertg," in *2016 IEEE 16th International Conference on Environment and Electrical Engineering (EEEIC)*, 2016, pp. 1–6.

[21] W. Niu, X. Huang, F. Yuan, N. Schofield, L. Xu, J. Chu, and W. Gu, "Sizing of energy system of a hybrid lithium battery rtg crane," *IEEE Transactions on Power Electronics*, vol. 32, no. 10, pp. 7837–7844, 2017.

[22] M. U. Mutarraf, Y. Terriche, M. Nasir, Y. Guan, C.-L. Su, J. C. Vasquez, and J. M. Guerrero, "A communication-less multimode control approach for adaptive power sharing in ship-based seaport microgrid," *IEEE Transactions on Transportation Electrification*, vol. 7, no. 4, pp. 3070–3082, 2021.

[23] K. Mahmud, M. S. Rahman, J. Ravishankar, M. J. Hossain, and J. M. Guerrero, "Real-time load and ancillary support for a remote island power system using electric boats," *IEEE Transactions on Industrial Informatics*, vol. 16, no. 3, pp. 1516–1528, 2020.

[24] L. Li, Y. Li, R. Liu, Y. Zhou, and E. Pan, "A two-stage stochastic programming for agv scheduling with random tasks and battery swapping in automated container terminals," *Transportation Research Part E: Logistics and Transportation Review*, vol. 174, p. 103110, 2023.

[25] A. Papavasiliou, S. S. Oren, and R. P. O'Neill, "Reserve requirements for wind power integration: A scenario-based stochastic programming framework," *IEEE Transactions on Power Systems*, vol. 26, no. 4, pp. 2197–2206, 2011.

[26] X. Chen, W. Wu, and B. Zhang, "Robust restoration method for active distribution networks," *IEEE Transactions on Power Systems*, vol. 31, no. 5, pp. 4005–4015, 2016.

[27] Y. Zhou, M. Shahidehpour, Z. Wei, Z. Li, G. Sun, and S. Chen, "Distributionally robust unit commitment in coordinated electricity and district heating networks," *IEEE Transactions on Power Systems*, vol. 35, no. 3, pp. 2155–2166, 2020.

[28] A. Lorca, X. A. Sun, E. Litvinov, and T. Zheng, "Multistage adaptive robust optimization for the unit commitment problem," *Operations Research*, vol. 64, no. 1, pp. 32–51, 2016.

[29] A. Bhattacharya, J. P. Kharoufeh, and B. Zeng, "Managing energy storage in microgrids: A multistage stochastic programming approach," *IEEE Transactions on Smart Grid*, vol. 9, no. 1, pp. 483–496, 2018.

[30] J. Zou, S. Ahmed, and X. A. Sun, "Stochastic dual dynamic integer programming," *Mathematical Programming*, vol. 175, pp. 461–502, 2019.

[31] Z. Li, P. Yang, Z. Zhao, and L. L. Lai, "Retrofit planning and flexible operation of coal-fired units using stochastic dual dynamic integer programming," *IEEE Transactions on Power Systems*, vol. 39, no. 1, pp. 2154–2169, 2024.

[32] Y. Shi, S. Dong, C. Guo, Z. Chen, and L. Wang, "Enhancing the flexibility of storage integrated power system by multi-stage robust dispatch," *IEEE Transactions on Power Systems*, vol. 36, no. 3, pp. 2314–2322, 2021.

[33] H. Xiong, M. Yan, F. Li, T. Ding, C. Guo, and Z. Li, "Resilience enhancement for distribution system with multiple non-anticipative uncertainties based on multi-stage dynamic programming," *IEEE Transactions on Smart Grid*, pp. 1–1, 2024.

[34] T. Ding, X. Zhang, R. Lu, M. Qu, M. Shahidehpour, Y. He, and T. Chen, "Multi-stage distributionally robust stochastic dual dynamic programming to multi-period economic dispatch with virtual energy storage," *IEEE Transactions on Sustainable Energy*, vol. 13, no. 1, pp. 146–158, 2022.

[35] Z. Li, P. Yang, Y. Guo, and G. Lu, "Medium-term multi-stage distributionally robust scheduling of hydro–wind–solar complementary systems in electricity markets considering multiple time-scale uncertainties," *Applied Energy*, vol. 347, p. 121371, 2023. [Online]. Available: https://www.sciencedirect.com/science/article/pii/S0306261923007353

[36] Y. Huang, W. Huang, N. Tai, C. Li, R. Li, and M. Yu, "A multistage distributionally robust optimization approach for generation dispatch with demand response under endogenous and exogenous uncertainties," *IET Generation, Transmission & Distribution*, vol. 17, no. 22, pp. 5041–5061, 2023.

[37] A. D. O. Dowson, D. P. Morton, "Bi-objective multistage stochastic linear programming," *Mathematical Programming*, vol. 196, pp. 907–933, 2022.

[38] Y. Huang, W. Huang, R. Li, and N. Tai, "Optimal operation of seaport integrated energy systems with coordination between logistic and energy systems," in *2023 IEEE/IAS Industrial and Commercial Power System Asia (ICPS Asia)*, 2023, pp. 2018–2024.
[39] Y. Luo, S. Fang, L. Kong, T. Niu, and R. Liao, "Dynamic power management of shipboard hybrid energy storage system under uncertain navigation conditions," *IEEE Transactions on Transportation Electrification*, pp. 1–1, 2023.
[40] M. Ehrgott, *Multicriteria Optimization*. Springer Berlin, Heidelberg, 2005.
[41] Y. Huang, "System data." [Online]. Available: https://github.com/YiwenHuangg/data

Yiwen Huang received the B.E. degree in electrical power engineering from Harbin Institute of Technology, Harbin, China, in 2020. He is currently working toward the Ph.D. degree with the Department of Power Electrical Engineering, Shanghai Jiao Tong University, Shanghai, China. His research interests include mathematical programming, machine learning, and transportation-power system operation.

Wentao Huang (Senior Member, IEEE) received the Ph.D. degree in electrical engineering from Shanghai Jiao Tong University, Shanghai, China, in 2015. He is currently a Professor with the Department of Power Electrical Engineering, Shanghai Jiao Tong University. His research interests include protection and control of active distribution systems, microgrids, smart grid, and renewable energy.

Tao Huang (Senior Member, IEEE) received the Ph.D. degree from Politecnico di Torino, Turin, Italy, in 2011. He is currently an Associate Professor with the Department of Energy, Politecnico di Torino. He is also an Adjunct Professor with Xihua University, Chengdu, China, and Polytechnic University of Henan, Jiaozuo, China. His research interests include vulnerability assessment, electricity markets, smart grids, active distribution network, and artificial intelligence in power systems.

Canbing Li (Senior Member, IEEE) received the B.E. and Ph.D. degrees from the Department of Electrical Engineering, Tsinghua University, Beijing, China, in 2001 and 2006, respectively. He is currently a Professor with Shanghai Jiao Tong University. His research interests include power systems, smart grid, renewable energy, with an emphasis on large-scale power system dispatch, economic and secure operation of power systems, energy efficiency and energy saving in smart grid, electric demand management of data centers, vehicle-to-grid technologies.

Ran Li (Member, IEEE) received the B.E. degrees in electrical power engineering from the University of Bath, Bath, U.K, and North China Electric Power University, Beijing, China, in 2011, and the Ph.D. degree from the University of Bath, Bath, U.K, in 2014. He is currently an Associate Professor with the Department of Power Electrical Engineering, Shanghai Jiao Tong University. His research interests include power system data analytics and power economics.

Nengling Tai (Senior Member, IEEE) received the B.E. and Ph.D. degrees in electrical engineering from the Huazhong University of Science and Technology, Wuhan, China, in 1994, and 2000, respectively. He is currently a Professor with the Department of Power Electrical Engineering, Shanghai Jiao Tong University, Shanghai, China. His research interests include the HVDC transmission system and smart grid.

Ettore Francesco Bompard received the Ph.D. degree in electrical engineering from Politecnico di Torino, Turin, Italy, in 1994. He is currently a Professor of Power Systems with the Department of Energy, Politecnico di Torino and a Scientific Director of the Energy Security Transition Lab @Energy Center, Torino. His research interests include electricity markets analysis and simulation, smart grids design and modeling, power system vulnerability assessment and security management, energy security, "science-based" support to policy decision-making, and data analytics applications to power systems.